An upscaled model for permeable biofilm in a thin channel and tube

David Landa-Marbán, Gunhild Bødtker, Kundan Kumar, Iuliu Sorin Pop, Florin Adrian Radu

UHasselt Computational Mathematics Preprint
Nr. UP-18-09

Oct. 16, 2018

An upscaled model for permeable biofilm in a thin channel and tube

David Landa-Marbán[1] Gunhild Bødtker[2] Kundan Kumar[1] Iuliu Sorin Pop[1,3]
Florin Adrian Radu[1]

[1] Department of Mathematics, Faculty of Mathematics and Natural Sciences, University of Bergen, Allégaten 41, P.O. Box 7803, 5020 Bergen, Norway.

[2] NORCE, P.O. Box 7800, N-5020, Bergen, Norway.

[3] Faculty of Sciences, Hasselt University, Campus Diepenbeek, Agoralaan building D, BE3590 Diepenbeek, Belgium.

Corresponding author: David Landa-Marbán (E-mail: David.Marban@uib.no)

Abstract

In this paper, we derive upscaled equations for modeling biofilm growth in porous media. The resulting macro-scale mathematical models consider permeable multi-species biofilm including water flow, transport, detachment, and reactions. We start with a pore-scale mathematical model for permeable biofilm formation. The biofilm is composed by extracellular polymeric substances (EPS), water, active bacteria, and dead bacteria. The free flow is described by the Stokes system and the water flux inside the biofilm by the Brikman equations. The nutrients are transported in the water phase by convection and diffusion. This pore-scale model includes variations of the biofilm composition and size due to reproduction of bacteria, production of EPS, death of bacteria, and shear forces. The model includes a water-biofilm interface between the free flow and the biofilm. Homogenization techniques are applied to obtain upscaled models in a thin channel and a tube. The resulting numerical computations are presented to compare the outcome of the effective (upscaled) models for the two different geometries.

Symbols

c	Nutrient concentration
C	Reference nutrient concentration
d	Biofilm height
D	Nutrient diffusion coefficient
E	Integration coefficient
F	Integration coefficient
G	Integration coefficient
h	Variable dependent on the biofilm height (channel)
H	Set-valued Heaviside graph
H^δ	Regularized set-valued Heaviside graph
i	Imaginary number
I	Identity matrix
J	Nutrient flux
J_ν	Bessel function of order ν of first kind
k	Permeability
K	Saturated hydraulic conductivity
k_{res}	Bacterial decay rate coefficient
k_{str}	Stress coefficient
k_n	Monod-half nutrient velocity coefficient
l	Height of thin channel
L	Pore length
M'	Matrix with flux water derivatives (tube)
$M^,$	Matrix with flux water derivatives (channel)
p	Pressure
P	Reference pressure
P_e	Péclet number
q	Water velocity

$\bar{q}$	Average water velocity (tube)
$\hat{q}$	Average water velocity (channel)
Q	Reference water velocity
r	Radial coordinate
R	Reaction term
S	Tangential shear stress
t	Time
T	Reference time
u	Velocity of the biomass
U	Reference biomass velocity
v	Darcy velocity
V	Integration coefficient
w	Variable dependent of the biofilm height (tube)
W	Integration coefficient
x	Cartesian coordinate
X	Integration coefficient
y	Cartesian coordinate
Y	Yield coefficient
Y_ν	Bessel function of order ν of second kind
z	Cartesian/Cylindrical coordinate
Greek symbols	
χ	General variable
δ	Small regularization parameter
ε	Dimensionless aspect ratio (channel)
η	Experimentally determined parameter
Γ	Space boundary
κ_c	Effective permeability (channel)
κ_t	Effective permeability (tube)
μ	Dynamic viscosity
μ_n	Maximum rate of nutrient utilization
η	Experimental determined parameter
ν	Unitary normal vector (interface)
ν_n	Interface velocity
Ω	Space domain
ϕ	Porosity of the porous medium
Φ	Growth velocity potential
ρ	Density
Σ	Sum of reaction terms
τ	Unitary tangential vector
θ	Volume fraction
υ	Unitary normal vector (wall)
ξ	Variable dependent of the permeability and water content (tube)
Ξ'	Space region (tube)
Ξ,	Space region (channel)
ε	Dimensionless aspect ratio (tube)
ρ	Tube radius
φ	Angular coordinate
Subscripts/superscripts	
a	Active bacteria
B	Biodegradation microbe
b	Biofilm
C	Channel
d	Dead bacteria
i	Input
ib	Input biofilm domain
iw	Input water domain
K	Biobarrier-forming microbe
l	Lower

m	Middle
o	Output
ob	Output biofilm domain
ow	Output water domain
e	EPS
s	Wall
T	Tube
u	Up
w	Water
wb	Water-biofilm (interface)
0	Initial

Abbreviations

EPS	Extracellular polymeric substance
MEOR	Microbial Enhanced Oil Recovery

1 Introduction

Biofilms are sessile communities of bacteria housed in a self-produced adhesive matrix consisting of extracellular polymeric substances (EPS), including polysaccharides, proteins, lipids, and DNA [1]. The proportion of EPS in biofilms is 50% to 90% of the total organic matter [8, 26]. Water is by far the largest component of the matrix, giving biofilms the nickname "stiff water" [9]. Biofilms provoke chronic bacterial infection, infection on medical devices, deterioration of water quality, and the contamination of food [12]. On the other hand, biofilms can be used for wastewater treatment and bioenergy production [16]. In microbial enhanced oil recovery (MEOR), one of the strategies is selective plugging, where bacteria are used to form biofilm in the high permeable zones to diverge the water flow and extract the oil located in the low permeable zones [20]. In wastewater treatment, one of the strategies consists in using biofilms to break down compounds which it is not desirable to discharge into the natural environment [5].

Two of the motivations to derive upscaled models are to describe the average behavior of the system in an accurate manner with relatively low computational effort compared to fully detailed calculations starting at the microscale [24] and to determine constitutive relationships [11]. We also refer to [19], and [21], where the authors upscale various pore-scale models for biofilm formation in perforated and strip geometries.

The present work builds on [14], where a pore-scale model is discussed. The model includes permeability and different biofilm components. This mathematical model is based on laboratory experiments performed by [15], where the biofilm was grown in micro-channels. Here we upscale this pore-scale model to derive one-dimensional effective equations, by investigating the limit as the ratio of the height to the length approaches to zero.

In this general context, the objective of the research reported in the present article is to obtain core-scale models for permeable biofilm in two different pore geometries. The motivation to choose these two geometries is because experiments are performed in the laboratory in different geometries [3, 15] and some porous media can be modeled as a stack of micro-tubes or micro-channels [24].

To summarize, the novel aspect in this work is in deriving core-scale models from a pore-scale model for a biofilm which is permeable to the flow and has a variable (in time and space) height. The fluid flow in the biofilm is modeled by the Brinkman equations, whereas in the remaining pore space the Stokes model is adopted. This is done for two different geometries. We derive analytical expressions for the upscaled quantities and provide numerical simulation results for the upscaled models in both cases.

The structure of this paper is as follows. In section 2, we describe the pore-scale biofilm model. In section 3, we present the dimensionless pore-scale biofilm model. In section 4, we perform formal homogenization on the model equations and obtain upscaled equations. In section 5, we compare the upscaled models with the upscaled model of [24] and with the well-known core-scale model of [6]. Also, we perform numerical simulations in the upscaled models and we compare the results for the percentage of biofilm coverage area and biofilm height for the two different effective models. Finally, in section 6 we present the conclusions.

2 Pore-Scale Model

The pore-scale mathematical model considered here follows ideas from [2] ,[24], and [7]. A detailed description of this model can be found in [14], where a comparison of laboratory measurements and numerical simulations is also presented.

The biofilm has four components: water, EPS, active, and dead bacteria ($j = \{w, e, a, d\}$). Let θ_j and ρ_j denote the volume fraction and the density of species j. The sum of volume fractions is constraint to 1 ($\theta_w + \theta_e + \theta_a + \theta_d = 1$). The biomass phases and water are assumed to be incompressible ($\partial_t \rho_j = 0$) and the biofilm layer is attached to the pore walls. Recalling that biofilms are formed mostly by water, the volume fraction of water θ_w is taken as a constant. Figure 1 shows schematically the phenomena considered for the biofilm formation.

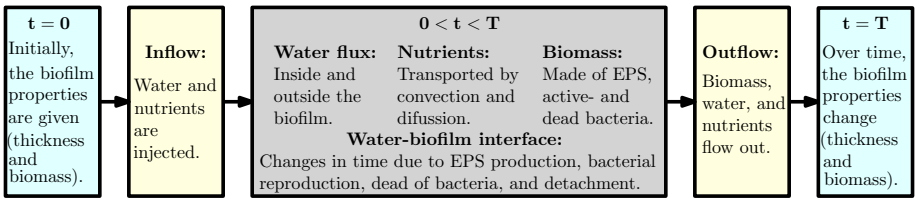

Figure 1: Conceptual pore-scale model showing the processes for the biofilm dynamics.

We consider two different pore geometries: a thin channel in Cartesian coordinates (x,y,z) and a tube in cylindrical coordinates (r,φ,z). In the first case, the pore has circular cross-section, and in the second a rectangular one. In both cases, the length is bigger than the cross-sectional diameter. In both cases, we assume a certain symmetry. For the cylindrical pore we assume that the processes are radially symmetric, hence there is no angular dependence (see Figure 2). For the thin channel, there are no changes in the x direction, so it can be reduced to a two-dimensional strip (see Figure Figure 8). This assumption is based on experiments, showing that when the width of the channel is much smaller than its height, the growing of the biofilm occurs only at the upper and lower walls [15]. We present in detail the upscaling of the model equations on the tube geometry. The upscaling on the channel geometry is shown in Appendix A. Figure 2 shows the different domains, boundaries, and interface in the pore with tubular geometry.

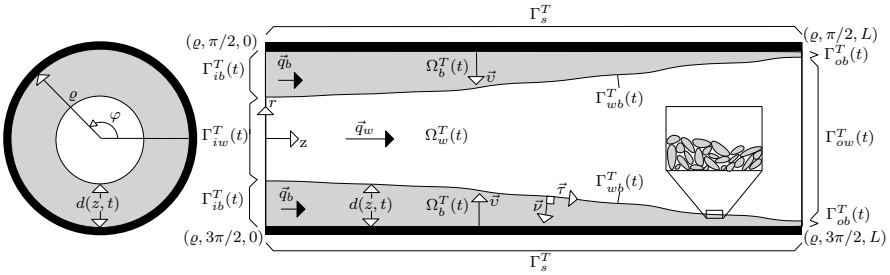

Figure 2: Pore of radius ρ and length L in cylindrical coordinates.

We consider a thin tube of radius ρ and length L,

$$\text{Tube} \qquad \Omega^T := [0,\rho]\times[0,2\pi)\times[0,L]. \tag{1}$$

The domain is occupied by the water and biofilm phases with the biofilm located along the tube walls. This leads to the following sub-domains in the tube:

$$\begin{aligned} \text{Water} \quad & \Omega_w^T(t) := \{\vec{r}\,|\, r\in[0,\rho-d(z,t)),\ \varphi\in\times[0,2\pi),\ z\in(0,L)\},\\ \text{Biofilm} \quad & \Omega_b^T(t) := \{\vec{r}\,|\, r\in(\rho-d(z,t),\rho),\ \varphi\in\times[0,2\pi),\ z\in(0,L)\}. \end{aligned} \tag{2}$$

The boundary of the tube consists of the wall, and the in- and outflow boundaries

$$\begin{aligned} \text{Wall} \quad & \Gamma_s^T := \{\rho\}\times[0,2\pi)\times[0,L],\\ \text{Inflow} \quad & \Gamma_i^T := [0,\rho]\times[0,2\pi)\times\{0\},\\ \text{Outflow} \quad & \Gamma_o^T := [0,\rho]\times[0,2\pi)\times\{L\}. \end{aligned} \tag{3}$$

The water domain has three boundary parts: the in- and outflow, and the interface between the water and the biofilm

$$\begin{aligned} \text{Water inflow} \quad & \Gamma_{iw}^T(t) := \{\vec{r}\,|\, r\in[0,\rho-d(z,t)),\ \varphi\in\times[0,2\pi),\ z=0\},\\ \text{Water outflow} \quad & \Gamma_{ow}^T(t) := \{\vec{r}\,|\, r\in[0,\rho-d(z,t)),\ \varphi\in\times[0,2\pi),\ z=L\},\\ \text{Water-biofilm interface} \quad & \Gamma_{wb}^T(t) := \{\vec{r}\,|\, r=\rho-d(z,t),\ \varphi\in\times[0,2\pi),\ z\in(0,L)\}. \end{aligned} \tag{4}$$

Similarly, for the biofilm one has the in- and outflow boundary parts, the water-biofilm interface Γ_{wb}^T, and the solid tube wall Γ_s^T

$$
\begin{array}{lrcl}
\text{Biofilm inflow} & \Gamma_{ib}^T(t) & := & \{\vec{r}|\ r \in (\rho - d(z,t), \rho),\ \varphi \in \times[0,2\pi),\ z = 0\}, \\
\text{Biofilm outflow} & \Gamma_{ob}^T(t) & := & \{\vec{r}|\ r \in (\rho - d(z,t), \rho),,\ \varphi \in \times[0,2\pi)\ z = L\}.
\end{array} \tag{5}
$$

The unit normal $\vec{\nu}$ pointing into the biofilm and the normal velocity of the interface v_n can be written in terms of the biofilm height d as [24]

$$
\begin{array}{lrcl}
\text{Unit normal} & \vec{\nu} & = & (1, \partial_z d)/\sqrt{1 + (\partial_z d)^2}, \qquad (6) \\
\text{Normal velocity} & v_n & = & -\partial_t d/\sqrt{1 + (\partial_z d)^2}. \qquad (7)
\end{array}
$$

Although the tube is a three-dimensional domain, recalling the rotational symmetry, we only write the $\hat{r}$ and $\hat{z}$ components of the vectors in order to reduce the length of the mathematical expressions.

The water flux is described by the Stokes equations

$$
\text{Stokes equations} \qquad \nabla \cdot \vec{q}_w = 0, \qquad \mu \Delta \vec{q}_w = \nabla p_w \qquad \text{in } \Omega_w^T(t), \tag{8}
$$

while the water flux inside the biofilm is described by the Brinkman equations

$$
\text{Brinkman equations} \qquad \nabla \cdot \vec{q}_b = 0, \qquad (\mu/\theta_w)\Delta \vec{q}_b - (\mu/k)\vec{q}_b = \nabla p_b \qquad \text{in } \Omega_b^T(t). \tag{9}
$$

Here p_w and p_b are the water pressures and $\vec{q}_w$ and $\vec{q}_b$ are the water velocities in the water domain and biofilm domain respectively; μ is the water viscosity (constant, not dependent on biofilm species), and k is the permeability of the biofilm (assumed isotropic). At the interface $\Gamma_{wb}^T(t)$ one has the continuity of the velocity and of the normal stress tensor, and at the wall we consider the no-slip boundary condition

$$
\begin{array}{lrcll}
\text{Continuity stress tensor} & \vec{\nu} \cdot (\mu \nabla \vec{q}_w - I p_w) & = & \vec{\nu} \cdot ((\mu/\theta_w)\nabla \vec{q}_b - I p_b) & \text{at } \Gamma_{wb}^T(t), \\
\text{Continuity velocities} & \vec{q}_w & = & \vec{q}_b & \text{at } \Gamma_{wb}^T(t), \\
\text{No-slip condition} & \vec{q}_b & = & \vec{0} & \text{at } \Gamma_s^T,
\end{array} \tag{10}
$$

where I is the identity matrix.

To model the nutrient transport and consumption, we let c_α ($\alpha \in \{w, b\}$) stand for the nutrient concentration in water or biofilm respectively, and D is the nutrient diffusion coefficient in water. Then, the nutrients in the water and the biofilm satisfy the convection-diffusion equation

$$
\begin{array}{lrcll}
\text{Nutrient mass balance in water} & \partial_t c_w + \nabla \cdot \vec{J}_w & = & 0 & \text{in } \Omega_w^T(t), \\
\text{Nutrient mass balance in biofilm} & \partial_t(\theta_w c_b) + \nabla \cdot \vec{J}_b & = & R_b & \text{in } \Omega_b^T(t),
\end{array} \tag{11}
$$

where $\vec{J}_w$ and $\vec{J}_b$ are given by

$$
\begin{array}{lrcl}
\text{Nutrient flux in water} & \vec{J}_w & = & -D\nabla c_w + \vec{q}_w c_w, \\
\text{Nutrient flux in biofilm} & \vec{J}_b & = & -\theta_w D \nabla c_b + \vec{q}_b c_b.
\end{array} \tag{12}
$$

Further at $\Gamma_{wb}^T(t)$ we impose the mass conservation and the continuity of the concentration, and at the solid wall Γ_s^T the normal flux is 0

$$
\begin{array}{lrcll}
\text{Mass conservation} & (\vec{J}_b - \vec{J}_w) \cdot \vec{\nu} & = & v_n(\theta_w c_b - c_w) & \text{at } \Gamma_{wb}^T(t), \\
\text{Continuity of the concentration} & \theta_w c_b & = & c_w & \text{at } \Gamma_{wb}^T(t), \\
\text{Normal flux condition} & \vec{\upsilon} \cdot \vec{J}_b & = & 0 & \text{at } \Gamma_s^T,
\end{array} \tag{13}
$$

where $\vec{\upsilon}$ is the normal vector on the pore wall. The reaction term R_b for the consumption of nutrients is given by

$$\text{Nutrient consumption rate} \qquad R_b = -\mu_n \theta_a \rho_a c_b/(k_n + c_b), \tag{14}$$

where μ_n is the maximum rate of nutrient consumption and k_n is the Monod-half nutrient velocity coefficient.

To model the movement of the biomass components due to reproduction, production of EPS, and dead of active bacteria, we consider the following equations [2, 14]

$$\begin{array}{lrcll} \text{Potential equation} & \nabla\cdot\vec{u} & = & (1-\theta_w)^{-1}\Sigma_i(R_i/\rho_i),\ i\in\{e,a,d\} & \text{in } \Omega_b^T(t), \\ \text{Velocity of biomass} & \vec{u} & = & -\nabla\Phi & \text{in } \Omega_b^T(t), \\ \text{Reference potential} & \Phi & = & 0 & \text{at } \Gamma_{wb}^T(t), \\ \text{Wall condition} & \vec{v}\cdot\nabla\Phi & = & 0 & \text{at } \Gamma_s^T. \end{array} \tag{15}$$

where $\vec{u}$ is the velocity of the biomass and Φ is the growth velocity potential. The growth velocity potential is set to zero at the interface $\Gamma_{wb}^T(t)$.

For each of the biomass components, we assume mass conservation [2]

$$\begin{array}{lrcll} \text{Conservation of mass} & \rho_i\partial_t\theta_i + \rho_i\nabla\cdot(\theta_i\vec{u}) & = & R_i,\ i\in\{e,a,d\} & \text{in } \Omega_b^T(t), \\ \text{Detached components} & \vec{v}\cdot\nabla\theta_i & = & 0 & \text{at } \Gamma_{wb}^T(t), \\ \text{Wall condition} & \vec{v}\cdot\nabla\theta_i & = & 0 & \text{at } \Gamma_s^T. \end{array} \tag{16}$$

The reaction terms for the biomass components are given by

$$\begin{array}{lrcl} \text{Dead bacterial rate} & R_d & = & k_{res}\theta_a\rho_a, \\ \text{Active bacterial rate} & R_a & = & -Y_a\mu_n\theta_a\rho_a c_b/(k_n+c_b) - k_{res}\theta_a\rho_a, \\ \text{EPS rate} & R_e & = & -Y_e\mu_n\theta_a\rho_a c_b/(k_n+c_b), \end{array} \tag{17}$$

where Y_e and Y_a are yield coefficients and k_{res} is the bacterial decay rate.

The water-biofilm interface changes in time due to the water flux provoking detachment of components and the changes inside the biofilm. Thus, the normal velocity of the interface is given by [24]

$$\text{Normal velocity} \qquad v_n = \begin{cases} [\vec{v}\cdot\vec{u}]_+, & \text{if } d = l, \\ \vec{v}\cdot\vec{u} + k_{str}S, & \text{if } 0 < d < l, \quad \text{at } \Gamma_{wb}^T(t). \\ 0, & \text{if } d = 0, \end{cases} \tag{18}$$

Here k_{str} is the stress coefficients and S is the tangential shear stress, given by

$$\text{Tangential shear stress} \qquad S := ||(I - \vec{v}\vec{v}^T)\mu(\nabla\vec{q}_w + \nabla\vec{q}_w^T)\vec{v}||. \tag{19}$$

This pore-scale model can be extended to consider more complex systems. For example, one can add different kind of nutrients, different active bacteria species in the biofilm, or bacterial attachment.

3 Non-dimensional model

Before seeking an effective model, we bring the mathematical equations to a non-dimensional form. To this aim, we introduce the reference time T, length L, radius ρ, water velocity $Q := L/T$, biomass velocity U, pressure P, and concentration C. The thin tube is characterized by the ratio of its radius to the length $\varepsilon := \rho/L$, which is called the dimensionless aspect ratio. We define the following dimensionless coordinates

$$t := \frac{t}{T}, \qquad r := \frac{r}{\rho}, \qquad z := \frac{z}{L}.$$

The non-dimensional biofilm height is given by $d^\varepsilon := d/\rho$. In view of the scaling, the space domains (1)-(2) for the non-dimensional formulation become

$$
\begin{array}{lrcl}
\text{Tube} & \Omega^{T,\varepsilon} & := & [0,1]\times[0,2\pi)\times[0,1], \\
\text{Water} & \Omega_w^{T,\varepsilon}(t) & := & \{\vec{r}|\ r\in[0,1-d^\varepsilon(z,t)),\ \varphi\in\times[0,2\pi),\ z\in(0,1)\}, \\
\text{Biofilm} & \Omega_b^{T,\varepsilon}(t) & := & \{\vec{r}|\ r\in(1-d^\varepsilon(z,t),1),\ \varphi\in\times[0,2\pi),\ z\in(0,1)\},
\end{array}
$$

and the boundaries and interface become (3-5)

$$
\begin{array}{lrcl}
\text{Inflow} & \Gamma_i^{T,\varepsilon} & := & [0,1]\times[0,2\pi)\times\{0\}, \\
\text{Outflow} & \Gamma_o^{T,\varepsilon} & := & [0,1]\times[0,2\pi)\times\{1\}, \\
\text{Water inflow} & \Gamma_{iw}^{T,\varepsilon}(t) & := & \{\vec{r}|\ r\in[0,1-d^\varepsilon(z,t)),\ \varphi\in\times[0,2\pi),\ z=0\}, \\
\text{Water outflow} & \Gamma_{ow}^{T,\varepsilon}(t) & := & \{\vec{r}|\ r\in[0,1-d^\varepsilon(z,t)),\ \varphi\in\times[0,2\pi),\ z=1\}, \\
\text{Water-biofilm interface} & \Gamma_{wb}^{T,\varepsilon}(t) & := & \{\vec{r}|\ r=1-d^\varepsilon(z,t),\ \varphi\in\times[0,2\pi),\ z\in(0,1)\}, \\
\text{Biofilm inflow} & \Gamma_{ib}^{T,\varepsilon}(t) & := & \{\vec{r}|\ r\in(1-d^\varepsilon(z,t),1),\ \varphi\in\times[0,2\pi),\ z=0\}, \\
\text{Biofilm outflow} & \Gamma_{ob}^{T,\varepsilon}(t) & := & \{\vec{r}|\ r\in(1-d^\varepsilon(z,t),1),\ \varphi\in\times[0,2\pi),\ z=1\}, \\
\text{Wall} & \Gamma_s^{T,\varepsilon} & := & \{\rho\}\times[0,2\pi)\times(0,1).
\end{array}
$$

The non-dimensional unit normal (6) is given by

$$
\vec{\nu}^\varepsilon(r,z)=(1,\varepsilon\partial_z d^\varepsilon)/\sqrt{1+(\varepsilon\partial_z d^\varepsilon)^2}.
$$

We notice that a factor of ε appears in the second component of the non-dimensional unit normal, as a result of the upscaling of the coordinates

$$
\partial_z d=\frac{1}{L}\frac{\partial}{\partial z}\left(\rho\frac{d}{\rho}\right)=\frac{1}{L}\frac{\partial}{\partial z}(\rho d^\varepsilon)=\varepsilon\partial_z d^\varepsilon.
$$

We recall that due to the radial symmetry we have omitted the dependence of φ in the vector variables to reduce the length of the manuscript ($\vec{\nu}^\varepsilon(r,\varphi,z)=\vec{\nu}^\varepsilon(r,z)$). The non-dimensional nutrient concentrations and densities are given by

$$
c_w^\varepsilon:=\frac{c_w}{C},\qquad c_b^\varepsilon:=\frac{c_b}{C},\qquad \rho_i':=\frac{\rho_i}{C}\qquad i\in\{e,a,d\}.
$$

The water velocities are given by

$$
\vec{q}_w^\varepsilon(r,z)=(q_w^{\varepsilon(r)},\,q_w^{\varepsilon(z)}):=\left(\frac{q_w^{(r)}}{\varepsilon Q},\frac{q_w^{(z)}}{Q}\right),\qquad \vec{q}_b^\varepsilon(r,z)=(q_b^{\varepsilon(r)},\,q_b^{\varepsilon(z)}):=\left(\frac{q_b^{(r)}}{\varepsilon Q},\frac{q_b^{(z)}}{Q}\right),
$$

and the biomass velocity is given by

$$
\vec{u}^\varepsilon(r,z)=(u^{\varepsilon(r)},\,u^{\varepsilon(z)}):=\left(\frac{u^{(r)}}{\varepsilon U},\frac{u^{(z)}}{U}\right).
$$

Here, we assume that the velocities in the radial direction are of the order ρ/T. Hence, they scale by $1/\varepsilon$ when compared to the longitudinal velocities. The biomass volume fractions are dimensionless; therefore, in the non-dimensional model we simply define $\theta_i^\varepsilon:=\theta_i$, $i\in\{e,a,d\}$. Finally, the pressures and growth velocity potential become

$$
p_w^\varepsilon:=\frac{p_w}{P},\qquad p_b^\varepsilon:=\frac{p_b}{P},\qquad \Phi^\varepsilon:=\frac{\Phi}{UL\varepsilon^2}.
$$

We observe that the growth velocity potential Φ is scaled by $1/\varepsilon^2$ in order to have the biomass velocities in the radial direction of the order ρ/T [**?**, see]]Noorden:Article:2010.

We define the following dimensionless parameters

$$
P_e':=\frac{QL}{D},\ \mu_n':=T\mu_n,\ k_n':=\frac{k_n}{C},\ k':=\frac{k}{\rho^2},\ \mu':=\frac{\mu LQ}{\rho^2 P},\ k_{str}':=\frac{Pk_{str}}{U},\ k_{res}':=Tk_{res}.
$$

In this way, the dimensionless system of equations for the water flux (8-10) takes the form

$$\frac{1}{r}\partial_r(rq_w^{\varepsilon(r)})+\partial_z q_w^{\varepsilon(z)} = 0 \quad \text{in } \Omega_w^{T,\varepsilon}(t), \tag{20}$$

$$\mu'(\frac{1}{r}\partial_r(r\partial_r q_w^{\varepsilon(r)})+\varepsilon^2\partial_z^2 q_w^{\varepsilon(r)}-\frac{q_w^{\varepsilon(r)}}{r^2}) = \varepsilon^{-2}\partial_r p_w^{\varepsilon} \quad \text{in } \Omega_w^{T,\varepsilon}(t), \tag{21}$$

$$\mu'(\frac{1}{r}\partial_r(r\partial_r q_w^{\varepsilon(z)})+\varepsilon^2\partial_z^2 q_w^{\varepsilon(z)}) = \partial_z p_w^{\varepsilon} \quad \text{in } \Omega_w^{T,\varepsilon}(t), \tag{22}$$

$$\frac{1}{r}\partial_r(rq_b^{\varepsilon(r)})+\partial_z q_b^{\varepsilon(z)} = 0 \quad \text{in } \Omega_b^{T,\varepsilon}(t), \tag{23}$$

$$\frac{\mu'}{\theta_w}(\frac{1}{r}\partial_r(r\partial_r q_b^{\varepsilon(r)})+\varepsilon^2\partial_z^2 q_b^{\varepsilon(r)}-\frac{q_b^{\varepsilon(r)}}{r^2}) = \varepsilon^{-2}\partial_r p_b^{\varepsilon} \quad \text{in } \Omega_b^{T,\varepsilon}(t), \tag{24}$$

$$\frac{\mu'}{\theta_w}(\frac{1}{r}\partial_r(r\partial_r q_b^{\varepsilon(z)})+\varepsilon^2\partial_z^2 q_b^{\varepsilon(z)}) = \frac{\mu'}{k'}(q_b^{\varepsilon(r)}, q_b^{\varepsilon(z)})+\partial_z p_b^{\varepsilon} \quad \text{in } \Omega_b^{T,\varepsilon}(t), \tag{25}$$

$$\nu^{(z)}(\mu'\partial_z q_w^{\varepsilon(z)}-p_w^{\varepsilon}-\frac{\mu'}{\theta_w}\partial_z q_b^{\varepsilon(z)}+p_b^{\varepsilon}) = \varepsilon\nu^{(r)}(\frac{\mu'}{\theta_w}\partial_z q_b^{\varepsilon(r)}-\mu'\partial_z q_w^{\varepsilon(r)}) \text{ at } \Gamma_{wb}^{T,\varepsilon}(t), \tag{26}$$

$$\varepsilon\nu^{(r)}(\frac{\mu'}{\theta_w}\partial_r q_b^{\varepsilon(r)}-p_b^{\varepsilon}-\mu'\partial_r q_w^{\varepsilon(r)}+p_w^{\varepsilon}) = \nu^{(z)}(\mu'\partial_r q_w^{\varepsilon(z)}-\frac{\mu'}{\theta_w}\partial_r q_b^{\varepsilon(z)}) \text{ at } \Gamma_{wb}^{T,\varepsilon}(t), \tag{27}$$

$$(q_w^{\varepsilon(r)}, q_w^{\varepsilon(z)}) = (q_b^{\varepsilon(r)}, q_b^{\varepsilon(z)}) \quad \text{at } \Gamma_{wb}^{T,\varepsilon}(t), \tag{28}$$

$$(q_w^{\varepsilon(r)}, q_w^{\varepsilon(z)}) = (0, 0) \quad \text{at } \Gamma_s^{T,\varepsilon}, \tag{29}$$

where (20-22) are the dimensionless Stokes equations, (23-25) are the dimensionless Brinkman equations, (26-28) are the dimensionless interface conditions, and (29) is the dimensionless condition on the wall.

The dimensionless equations for the transport of nutrients (11-13) in the water and biofilm are given by

$$\partial_t c_w^{\varepsilon}-\frac{1}{P_e'}(\frac{\varepsilon^{-2}}{r}\partial_r(r\partial_r c_w^{\varepsilon})+\partial_z^2 c_w^{\varepsilon})+\frac{1}{r}\partial_r(rq_w^{\varepsilon(r)}c_w^{\varepsilon})+\partial_z(q_w^{\varepsilon(z)}c_w^{\varepsilon}) = 0 \quad \text{in } \Omega_w^{T,\varepsilon}(t), \tag{30}$$

$$\partial_t(\theta_w c_b^{\varepsilon})-\frac{\theta_w}{P_e'}(\frac{\varepsilon^{-2}}{r}\partial_r(r\partial_r c_b^{\varepsilon})+\partial_z^2 c_b^{\varepsilon})+\frac{1}{r}\partial_r(rq_b^{\varepsilon(r)}c_b^{\varepsilon})+\partial_z(q_b^{\varepsilon(z)}c_b^{\varepsilon}) = R_b^{\varepsilon} \quad \text{in } \Omega_b^{T,\varepsilon}(t), \tag{31}$$

$$-\frac{1}{P_e'\varepsilon^2}(\partial_r c_w^{\varepsilon}-\theta_w\partial_r c_b^{\varepsilon})-(c_b^{\varepsilon}q_b^{\varepsilon(r)}-c_w^{\varepsilon}q_w^{\varepsilon(r)})+\partial_t d^{\varepsilon}(\theta_w c_b^{\varepsilon}-c_w^{\varepsilon})$$
$$+\frac{\partial_z d^{\varepsilon}}{P_e'}(\partial_z c_w^{\varepsilon}-\theta_w\partial_z c_b^{\varepsilon})+\partial_z d^{\varepsilon}(c_b^{\varepsilon}q_b^{\varepsilon(z)}-c_w^{\varepsilon}q_w^{\varepsilon(z)}) = 0 \quad \text{at } \Gamma_{wb}^{T,\varepsilon}(t), \tag{32}$$

$$\theta_w c_b^{\varepsilon} = c_w^{\varepsilon} \quad \text{at } \Gamma_{wb}^{T,\varepsilon}(t), \tag{33}$$

$$\partial_r c_b^{\varepsilon} = 0 \quad \text{at } \Gamma_s^{T,\varepsilon}(t), \tag{34}$$

where (30) is the dimensionless transport equation of nutrients in the water domain, (31) is the dimensionless transport equation of nutrients in the biofilm domain, (32)-(33) are the dimensionless coupling conditions at the interface, and (34) is the dimensionless condition on the wall. The dimensionless reaction rate (14) for the consumption of nutrients is given by

$$R_b^{\varepsilon} = -\mu_n'\theta_a^{\varepsilon}\rho_a'\frac{c_b^{\varepsilon}}{k_n'+c_b^{\varepsilon}}.$$

The equations for the growth velocity potential (15) become

$$\frac{U}{Q}(\frac{1}{r}\partial_r(ru^{\varepsilon(r)})+\partial_z u^{\varepsilon(z)}) = \Sigma^{\varepsilon} \quad \text{in } \Omega_b^{T,\varepsilon}(t), \tag{35}$$

$$(u^{\varepsilon(r)}, u^{\varepsilon(z)}) = -(\partial_r\Phi^{\varepsilon}, \varepsilon^2\partial_z\Phi^{\varepsilon}) \quad \text{in } \Omega_b^{T,\varepsilon}(t), \tag{36}$$

$$\Phi^{\varepsilon} = 0 \quad \text{at } \Gamma_{wb}^{T,\varepsilon}(t), \tag{37}$$

$$\partial_r\Phi^{\varepsilon} = 0 \quad \text{at } \Gamma_s^{T,\varepsilon}, \tag{38}$$

where (35)-(36) are the dimensionless equations for the biomass growth velocity potential, (37) is the dimensionless reference potential at the interface, and (38) is the dimensionless condition on the wall. We define the dimensionless sum of the biomass reaction terms as

$$\Sigma^{\varepsilon} := \left(\frac{\rho_a'}{\rho_e'}Y_e + Y_a\right)\mu_n'\theta_a^{\varepsilon}\frac{c_b^{\varepsilon}}{k_n' + c_b^{\varepsilon}} + \left(\frac{\rho_a'}{\rho_d'} - 1\right)k_{res}'\theta_a^{\varepsilon}.$$

The equations for the biomass components (16) become

$$\begin{aligned}
\partial_t\theta_e^{\varepsilon} + \frac{U}{Q}(u^{\varepsilon(r)}\partial_r\theta_e^{\varepsilon} + u^{\varepsilon(z)}\partial_z\theta_e^{\varepsilon}) &= Y_e\mu_n'\theta_a^{\varepsilon}\frac{\rho_a'}{\rho_e'}\frac{c_b^{\varepsilon}}{k_n' + c_b^{\varepsilon}} - \theta_e^{\varepsilon}\Sigma^{\varepsilon} && \text{in } \Omega_b^{T,\varepsilon}(t), && (39)\\
\partial_t\theta_a^{\varepsilon} + \frac{U}{Q}(u^{\varepsilon(r)}\partial_r\theta_a^{\varepsilon} + u^{\varepsilon(z)}\partial_z\theta_a^{\varepsilon}) &= Y_a\mu_n'\theta_a^{\varepsilon}\frac{c_b^{\varepsilon}}{k_n' + c_b^{\varepsilon}} - k_{res}'\theta_a^{\varepsilon} - \theta_a^{\varepsilon}\Sigma^{\varepsilon} && \text{in } \Omega_b^{T,\varepsilon}(t), && (40)\\
\partial_t\theta_d^{\varepsilon} + \frac{U}{Q}(u^{\varepsilon(r)}\partial_r\theta_d^{\varepsilon} + u^{\varepsilon(z)}\partial_z\theta_d^{\varepsilon}) &= k_{res}'\frac{\rho_a'}{\rho_d'}\theta_a^{\varepsilon} - \theta_d^{\varepsilon}\Sigma^{\varepsilon} && \text{in } \Omega_b^{T,\varepsilon}(t), && (41)\\
-\partial_r\theta_i + \varepsilon\partial_z d^{\varepsilon}\partial_z\theta_i &= 0 \quad i \in \{e,a,d\} && \text{at } \Gamma_{wb}^{T,\varepsilon}(t), && (42)\\
\partial_r\theta_i &= 0 \quad i \in \{e,a,d\} && \text{at } \Gamma_s^{T,\varepsilon}, && (43)
\end{aligned}$$

where (39-41) are the dimensionless conservation of mass equations for the biomass components, (42) is the dimensionless condition at the interface, and (43) is the dimensionless condition on the wall.

The dimensionless biofilm height (18)-(19) is given by

$$\partial_t d^{\varepsilon} = \begin{cases} [-\frac{U}{Q}(-u^{\varepsilon(r)} + \partial_z d^{\varepsilon}u^{\varepsilon(z)})]_+, & \text{if } d = 1,\\ -\sqrt{1 + (\varepsilon\partial_z d^{\varepsilon})^2}\varepsilon k_{str}'S' - \frac{U}{Q}(-u^{\varepsilon(r)} + \partial_z d^{\varepsilon}u^{\varepsilon(z)}), & \text{if } 0 < d < 1, \quad \text{at } \Gamma_{wb}^{T,\varepsilon}(t).\\ 0, & \text{if } d = 0, \end{cases} \tag{44}$$

The dimensionless tangential shear stress (19) is given by

$$S' = ||(I - \nu^{\varepsilon}\nu^{\varepsilon T})\mu' M'\nu^{\varepsilon}||, \tag{45}$$

where the matrix M' is given by

$$M' = \begin{pmatrix} \partial_r q_w^{\varepsilon(r)} & \varepsilon\partial_z q_w^{\varepsilon(r)} \\ \varepsilon^{-1}\partial_r q_w^{\varepsilon(z)} & \partial_z q_w^{\varepsilon(z)} \end{pmatrix}. \tag{46}$$

4 Upscaling

The pore-scale mathematical model describes the biofilm formation in a three-dimensional domain. When the length of the tube is much larger than its radius, it is possible to reduce the mathematical model from three to one dimension, letting the aspect ratio ε to approach zero. We perform a formal asymptotic expansion for the variables depending on ε, namely p_w^{ε}, p_b^{ε}, c_w^{ε}, c_b^{ε}, $\vec{q}_w^{\varepsilon}$, $\vec{q}_b^{\varepsilon}$, $\vec{u}^{\varepsilon}$, Φ^{ε}, θ_w^{ε}, θ_e^{ε}, θ_a^{ε}, θ_d^{ε} and d^{ε}. For all except d we assume

$$\chi^{\varepsilon}(\vec{r},t) = \chi_0(\vec{r},t) + \varepsilon\chi_1(\vec{r},t) + O(\varepsilon^2).$$

The corresponding asymptotic expansion of d is

$$d^{\varepsilon}(z,t) = d_0(z,t) + \varepsilon d_1(z,t) + O(\varepsilon^2).$$

In [24], [13], and [4], the authors present upscaled models for pore-scale mathematical models for reactive flows. Following the same ideas, we show how to obtain the corresponding upscaled model in the tube pore geometry.

We define the average water flow as the following integral

$$\hat{q}(z,t) = \hat{q}_w(z,t) + \hat{q}_b(z,t) = \int_0^{2\pi}\left(\int_0^{1-d_0} q_{w,0}^{(z)}rdr + \int_{1-d_0}^{1} q_{b,0}^{(z)}rdr\right)d\varphi. \tag{47}$$

We consider the following space regions in the tube

$$\begin{aligned}
\Xi_w' &= \{\vec{r}|\ r \le 1 - d\ \wedge\ 0 \le \varphi < 2\pi\ \wedge\ z_1 \le z \le z_1 + \delta z\},\\
\Xi_b' &= \{\vec{r}|\ 1 - d \le r \le 1\ \wedge\ 0 \le \varphi < 2\pi\ \wedge\ z_1 \le z \le z_1 + \delta z\}.
\end{aligned}$$

These regions are a disk of radius $1-d$ and a ring of height d respectively; both of length δz. Integrating (20) and (23) over the previous regions and using the Gauss theorem, we obtain

$$\begin{aligned}0 = \quad & \int_{\Xi'_w} \nabla\cdot\vec{q}_w^{\,\varepsilon} dV + \int_{\Xi'_b} \nabla\cdot\vec{q}_b^{\,\varepsilon} dV = 2\pi\int_{z_1}^{z_1+\delta_z} \vec{q}_w^{\,\varepsilon}\cdot\vec{\nu}\big|_{r=(1-d^\varepsilon)} dz \\ & +2\pi\int_0^{1-d^\varepsilon} (q_w^{\varepsilon(z)}\big|_{z=z_1+\delta_z} - q_w^{\varepsilon(z)}\big|_{z=z_1}) r dr - 2\pi\int_{z_1}^{z_1+\delta_z} (\vec{q}_b^{\,\varepsilon}\cdot\vec{\nu}\big|_{r=1-d^\varepsilon)} + \vec{q}_b^{\,\varepsilon}\cdot\vec{\nu}\big|_{r=1}) dz \\ & +2\pi\int_{1-d^\varepsilon}^1 (q_b^{\varepsilon(z)}\big|_{z=z_1+\delta_z} - q_b^{\varepsilon(z)}\big|_{z=z_1}) r dr.\end{aligned}$$

Recalling the no-slip condition for the water flux on the wall (29) and the continuity of fluxes at the interface (28), the previous equation becomes

$$\int_0^{1-d^\varepsilon} (q_w^{\varepsilon(z)}\big|_{z=z_1+\delta_z} - q_w^{\varepsilon(z)}\big|_{z=z_1}) r dr + \int_{1-d^\varepsilon}^1 (q_b^{\varepsilon(z)}\big|_{z=z_1+\delta_z} - q_b^{\varepsilon(z)}\big|_{z=z_1}) r dr = 0.$$

Dividing the previous equation by δ_z and letting δ_z approach zero, we obtain for the lowest-order terms in ε

$$\partial_z \hat{q} = \partial_z \hat{q}_w(z,t) + \partial_z \hat{q}_b(z,t) = 0,$$

where we have used the definition of the average water flow (47).

The lowest order terms in the Stokes model (20-22) lead to

$$\frac{1}{r}\partial_r(r q_{w,0}^{(r)}) + \partial_z q_{w,0}^{(z)} = 0, \qquad \partial_r p_{w,0} = 0, \qquad \frac{\mu'}{r}\partial_r(r\partial_r q_{w,0}^{(z)}) = \partial_z p_{w,0}. \tag{48}$$

From (48b), we conclude that $p_{w,0}$ does not depend on the r coordinate. Analogous, for the Brinkman model (23-25), the lower-order terms in ε give

$$\frac{1}{r}\partial_r(r q_{b,0}^{(r)}) + \partial_z q_{b,0}^{(z)} = 0, \qquad \partial_r p_{b,0} = 0, \qquad \frac{\mu'}{r\theta_w}\partial_r(r\partial_r q_{b,0}^{(z)}) - \frac{\mu'}{k'} q_{b,0}^{(z)} = \partial_z p_{b,0}. \tag{49}$$

From (49b), we conclude that $p_{b,0}$ does not depend on the r coordinate. Since $p_{w,0}$ and $p_{b,0}$ do not depend on the r coordinate, from (27) we conclude that $p_{w,0} = p_{b,0}$ at the biofilm-water interface, resulting in $p_{w,0}(z,t) = p_{b,0}(z,t) := p_0(z,t)$. We turn our attention to equations (48c) and (49c). It is possible to find solutions for $q_{w,0}^{(z)}$ and $q_{b,0}^{(z)}$ integrating twice with respect to r both equations and in addition using the symmetry, interface, and boundary conditions (26-29). After integration, we get

$$q_{w,0}^{(z)} = \left(\frac{r^2}{4} + E\right)\frac{\partial_z p_0}{\mu'}, \tag{50}$$

$$q_{b,0}^{(z)} = \left(F J_0(\xi r) + G Y_0(-\xi r) - k'\right)\frac{\partial_z p_0}{\mu'}, \tag{51}$$

where $J_\nu(z)$ and $Y_\nu(z)$ are the Bessel function of order ν of first and second kind respectively [**?**, see]]Olver:Book:2012. The coefficients appearing in (50)-(51) are

$$\begin{aligned}E = \quad & \frac{2w\theta_w(J_0(s)Y_0(-\xi w) - J_0(\xi w)Y_0(-s)) + \xi k'(J_0(\xi w)Y_1(-\xi w) + Y_0(-\xi w)J_1(\xi w))}{4(\xi J_0(\xi)Y_1(-\xi w) + \xi Y_0(-\xi)J_1(\xi w))} \\ & -\frac{\xi(4k' + w^2)(J_0(\xi)Y_1(-\xi w) + Y_0(-\xi)J_1(\xi w))}{4(\xi J_0(\xi)Y_1(-\xi w) + \xi Y_0(-\xi)J_1(\xi w))}, \\ F = \quad & \frac{2k'\xi Y_1(-\xi w) + w\theta_w Y_0(-\xi)}{2(\xi J_0(\xi)Y_1(-\xi w) + \xi Y_0(-\xi)J_1(\xi w))}, \\ G = \quad & \frac{2k'\xi J_1(\xi w) + w\theta_w J_0(\xi)}{2(\xi J_0(\xi)Y_1(-\xi w) + \xi Y_0(-\xi)J_1(\xi w))}, \\ w = \quad & 1 - d_0, \\ \xi = \quad & i\sqrt{\theta_w/k'},\end{aligned}$$

where i is the imaginary number. We remark that most of the mathematical commercial software includes the Bessel

functions; therefore, it is easy to use the above expression. Also, although the Bessel functions are evaluated with complex numbers, both fluxes $q_{w,0}^{(z)}$ and $q_{b,0}^{(z)}$ are given by real numbers.

To obtain the average water flow defined in (47), we integrate (50) and (51) as follow

$$\begin{aligned}\bar{q} = \quad & \frac{\partial_z p_0}{\mu'}\int_0^{2\pi}\left(\int_0^{1-d_0}\left(\frac{r^2}{4}+E\right)rdr\right.\\ & \left.+\int_{1-d_0}^{1}\left(FJ_0\left(ri\sqrt{\frac{\theta_w}{k'}}\right)+GY_0\left(-ri\sqrt{\frac{\theta_w}{k'}}\right)-k'\right)rdr\right)d\varphi\\ = \quad & 2\pi\left(\frac{(1-d_0)^4+8E(1-d_0)^2}{16}+i\sqrt{\frac{k'}{\theta_w}}\left(FY_1\left(-i\sqrt{\frac{\theta_w}{k'}}\right)-GJ_1\left(i\sqrt{\frac{\theta_w}{k'}}\right)\right.\right.\\ & -F(1-d_0)Y_1\left(-(1-d_0)i\sqrt{\frac{\theta_w}{k'}}\right)+G(1-d_0)J_1\left((1-d_0)i\sqrt{\frac{\theta_w}{k'}}\right)\Big)\\ & \left.-k'\frac{1-(1-d_0)^2}{2}\right)\frac{\partial_z p_0}{\mu'}.\end{aligned}$$

This gives the Darcy law

$$\bar{q} = -\frac{\kappa_t(d_0)}{\mu'}\partial_z p_0,$$

where $\kappa_t(d_0)$ is the effective permeability given by

$$\begin{aligned}\kappa_t(d_0) = \quad & -2\pi\left(\frac{(1-d_0)^4+8E(1-d_0)^2}{16}+i\sqrt{\frac{k'}{\theta_w}}\left(FY_1\left(-i\sqrt{\frac{\theta_w}{k'}}\right)-GJ_1\left(i\sqrt{\frac{\theta_w}{k'}}\right)\right.\right.\\ & -F(1-d_0)Y_1\left(-(1-d_0)i\sqrt{\frac{\theta_w}{k'}}\right)+G(1-d_0)J_1\left((1-d_0)i\sqrt{\frac{\theta_w}{k'}}\right)\Big)\\ & \left.-k'\frac{1-(1-d_0)^2}{2}\right).\end{aligned}$$

which changes according to the biofilm height d_0.

The growth velocity potential equations (35) and (36) for the lower-order terms in ε are

$$\frac{U}{Q}\left(\frac{1}{r}\partial_r(ru_0^{(r)})+\partial_z u_0^{(z)}\right)=\Sigma_0, \qquad u_0^{(r)}=-\partial_r\Phi_{b,0}, \qquad u_0^{(z)}=0, \tag{52}$$

where the boundary conditions for the interface (37) becomes $\Phi_{b,0}=0$ and wall (38) becomes $\partial_r\Phi_{b,0}=0$.

In dimensionless form, the volume fraction equations (39-41) are

$$\partial_t\theta_i^\varepsilon+\frac{U}{Q}(u^{\varepsilon(r)}\partial_r\theta_i^\varepsilon+u^{\varepsilon(z)}\partial_z\theta_i^\varepsilon)=R_i^\varepsilon-\theta_i^\varepsilon\Sigma^\varepsilon, \tag{53}$$

with $i=\{e,a,d\}$. We focus on biofilms where the biomass components change slightly along the r direction, resulting in the approximation $\theta_{i,0}(r,z,t)=\theta_{i,0}(z,t)$. Using (52c), the lower-order terms in (53) are

$$\partial_t\theta_{i,0}=R_{i,0}-\theta_{i,0}\Sigma_0.$$

Integrating (52a) over r and using the boundary conditions (37)-(38) one gets

$$u_0^{(r)}=\frac{Q}{2U}\Sigma_0(r-1). \tag{54}$$

For the nutrients, integrating (30) and (31) over r and φ yields

$$
\begin{aligned}
2\pi\int_0^{1-d^\varepsilon}\left(\partial_t c_w^\varepsilon-\frac{1}{P_e'}(\varepsilon^{-2}\frac{1}{r}\partial_r(r\partial_r c_w^\varepsilon)+\partial_z^2 c_w^\varepsilon)+\frac{1}{r}\partial_r(rq_w^{\varepsilon(r)}c_w^\varepsilon)+\partial_z(q_w^{\varepsilon(z)}c_w^\varepsilon)\right)rdr &= 0,\\
2\pi\int_{1-d^\varepsilon}^1\Bigg(\partial_t(\theta_w c_b^\varepsilon)-\frac{\theta_w}{P_e'}(\varepsilon^{-2}\frac{1}{r}\partial_r(r\partial_r c_b^\varepsilon)+\partial_z^2 c_b^\varepsilon)+\frac{1}{r}\partial_r(rq_b^{\varepsilon(r)}c_b^\varepsilon)+\partial_z(q_b^{\varepsilon(z)}c_b^\varepsilon)&\\
+\mu_n'\theta_a^\varepsilon\rho_a'\frac{c_b^\varepsilon}{k_n'+c_b^\varepsilon}\Bigg)rdr &= 0.
\end{aligned}
$$

Interchanging the integration and the differentiation operators, these equations become

$$
\begin{aligned}
\partial_t\left(\int_0^{1-d^\varepsilon}c_w^\varepsilon rdr\right)+\partial_t d^\varepsilon r c_w^\varepsilon\big|_{r=1-d^\varepsilon}-\partial_z\left(\int_0^{(1-d^\varepsilon)}\left(\frac{1}{P_e'}\partial_z c_w^\varepsilon-q_w^{\varepsilon(z)}c_w^\varepsilon\right)rdr\right)&\\
-\partial_z d^\varepsilon\left(\frac{1}{P_e'}r\partial_z c_w^\varepsilon-rq_w^{\varepsilon(z)}c_w^\varepsilon\right)\big|_{r=1-d^\varepsilon}+\left(\frac{1}{\varepsilon^2P_e'}r\partial_r c_w^\varepsilon-rq_w^{\varepsilon(r)}c_w^\varepsilon\right)\big|_{r=1-d^\varepsilon} &= 0,\\
\partial_t\left(\int_{(1-d^\varepsilon)}^1\theta_w c_b^\varepsilon rdr\right)-\partial_t d^\varepsilon\theta_w c_b^\varepsilon r\big|_{r=1-d^\varepsilon}&\\
-\partial_z\left(\int_{1-d^\varepsilon}^1\left(\frac{\theta_w}{P_e'}\partial_z c_b^\varepsilon-q_b^{\varepsilon(z)}c_b^\varepsilon\right)rdr\right)+\partial_z d^\varepsilon\left(\frac{\theta_w}{P_e'}r\partial_z c_b^\varepsilon-rq_b^{\varepsilon(z)}c_b^\varepsilon\right)\big|_{r=1-d^\varepsilon}&\\
-\left(\frac{\theta_w}{\varepsilon^2P_e'}r\partial_r c_b^\varepsilon-rq_b^{\varepsilon(r)}c_b^\varepsilon\right)\big|_{r=1-d^\varepsilon}+\mu_n'\rho_a'\theta_a^\varepsilon\int_{1-d^\varepsilon}^1\frac{c_b^\varepsilon}{k_n'+c_b^\varepsilon}rdr &= 0.
\end{aligned}
$$

Next, lower order terms in the equations for the conservation of nutrients (30) and (31) are

$$
\partial_r(r\partial_r c_{w,0})=0,\qquad \partial_r(r\partial_r(\theta_w c_{b,0}))=0.
$$

The interface coupling condition (32) becomes $\partial_r c_{w,0}=\partial_r(\theta_w c_{b,0})$ and (33) becomes $c_{w,0}=\theta_w c_{b,0}$, while the boundary condition on the wall (34) becomes $\partial_r(\theta_w c_{b,0})=0$. Therefore, we conclude that $c_{w,0}(z,t)=\theta_w c_{b,0}(z,t):=c_0(z,t)$. Then, using the aforementioned results, the equations for the nutrients can be written as

$$
\begin{aligned}
\frac{1}{2}\partial_t(c_0(1-d_0)^2)+\partial_t d_0 r c_0\big|_{r=1-d_0}-\frac{(1-d_0)^2}{2P_e'}\partial_z^2 c_0+c_0\int_0^{(1-d_0)}q_{w,0}^{(r)}rdr&\\
-\partial_z d_0\left(\frac{1}{P_e'}r\partial_z c_0-rq_w^{(z)}c_0\right)\big|_{r=1-d_0}+\left(\frac{1}{\varepsilon^2P_e'}r\partial_r c_0-rq_{w,0}^{(r)}c_0\right)\big|_{r=1-d_0} &= 0,\\
\frac{1}{2}\partial_t(c_0(1-(1-d_0)^2))-\partial_t d_0 r c_0\big|_{r=1-d_0}-\frac{1-(1-d_0)^2}{2P_e'}\partial_z^2 c_0&\\
+c_0\int_{1-d_0}^1 q_{b,0}^{(z)}rdr+\partial_z d_0\left(\frac{1}{P_e'}r\partial_z c_0-rq_{b,0}^{(z)}c_0\right)\big|_{r=1-d_0}&\\
-\left(\frac{1}{\varepsilon^2P_e'}r\partial_r c_0-q_{b,0}^{(r)}c_0\right)\big|_{r=1-d_0}+\frac{1-(1-d_0)^2}{2}\mu_n'\rho_a'\theta_{a,0}\frac{c_0}{k_n'+c_0} &= 0.
\end{aligned}
$$

Then, adding the both previous equations and using the interface condition (32), we finally obtain

$$
\partial_t c_0+\partial_z\left(c_0\hat{q}-\frac{1}{P_e'}\partial_z c_0\right)=-(1-(1-d_0)^2)\mu_n'\theta_{a,0}\rho_a'\frac{c_0}{k_n'+c_0}.
$$

We focus on the water-biofilm interface (44):

$$
\partial_t d^\varepsilon=\begin{cases}
[-\frac{U}{Q}(-u^{\varepsilon(r)}+\partial_z d^\varepsilon u^{\varepsilon(z)})]_+, & \text{if } d=1,\\
-\sqrt{1+(\varepsilon\partial_z d^\varepsilon)^2}\varepsilon k_{str}'S'-\frac{U}{Q}(-u^{\varepsilon(r)}+\partial_z d^\varepsilon u^{\varepsilon(z)}), & \text{if } 0<d<1,\\
0, & \text{if } d=0.
\end{cases}
\tag{55}
$$

Following [24], we regularize the formulation of (55). First we let H_0 and H_1 be the set-valued Heaviside graphs

$$H_0(d) := \begin{cases} \{0\}, & \text{if } d < 0, \\ [0,1], & \text{if } d = 0, \\ \{1\}, & \text{if } d > 0, \end{cases} \qquad H_1(d) := \begin{cases} \{1\}, & \text{if } d < 1, \\ [0,1], & \text{if } d = 1, \\ \{0\}, & \text{if } d > 1, \end{cases} \tag{56}$$

where we set $H_0(d^\varepsilon = 0) = 0$ and $H_1(d^\varepsilon = 1) = 0$. Observe that this choice guarantees that $\partial_t d^\varepsilon$ never becomes negative whenever $d^\varepsilon = 0$ and positive when $d^\varepsilon = 1$. Then, (55) is written as

$$\begin{aligned} \partial_t d^\varepsilon \in \quad & H_0(d^\varepsilon) H_1(d^\varepsilon) \Big(- \sqrt{1 + (\varepsilon \partial_z d^\varepsilon)^2}\, \varepsilon k'_{str} \mu' ||(I - \nu^\varepsilon \nu^{\varepsilon T}) M' \nu^\varepsilon|| \\ & - \frac{U}{Q}(-u^{\varepsilon(r)} + \partial_z d^\varepsilon u^{\varepsilon(z)}) \Big) + (1 - H_1(d^\varepsilon))[-\frac{U}{Q}(-u^{\varepsilon(r)} + \partial_z d^\varepsilon u^{\varepsilon(z)})]_+. \end{aligned} \tag{57}$$

For practical calculations, the multi-valued functions are replaced by regularized Heaviside functions, defined by

$$H_0^\delta(d) := \begin{cases} 0, & \text{if } d < 0, \\ d/\delta, & \text{if } d \in [0, \delta], \\ 1, & \text{if } d > \delta, \end{cases} \qquad H_1^\delta(d) := \begin{cases} 1, & \text{if } d < 1, \\ (1 + \delta - d)/\delta, & \text{if } d \in [1, 1+\delta], \\ 0, & \text{if } d > 1 + \delta, \end{cases} \tag{58}$$

where δ is a small regularization parameter. Then, we can write (57) as

$$\begin{aligned} \partial_t d^\varepsilon = \quad & H_0^\delta(d^\varepsilon) H_1^\delta(d^\varepsilon) \Big(- \sqrt{1 + (\varepsilon \partial_z d^\varepsilon)^2}\, \varepsilon k'_{str} \mu' ||(I - \nu^\varepsilon \nu^{\varepsilon T}) M' \nu^\varepsilon|| \\ & - \frac{U}{Q}(-u^{\varepsilon(r)} + \partial_z d^\varepsilon u^{\varepsilon(z)}) \Big) + (1 - H_1^\delta(d^\varepsilon))[-\frac{U}{Q}(-u^{\varepsilon(r)} + \partial_z d^\varepsilon u^{\varepsilon(z)})]_+. \end{aligned} \tag{59}$$

Using (45-46, 52c, 54) for the lower-order terms we have

$$\partial_t d^\varepsilon = H_0^\delta(d^\varepsilon) H_1^\delta(d^\varepsilon)(-k'_{str} \mu' |\partial_r q^{(z)}_{w,0}| + d_0 \Sigma_0/2) + (1 - H_1^\delta(d^\varepsilon))[-\Sigma_0/2]_+. \tag{60}$$

Using (50), we obtain

$$\partial_t d^\varepsilon = H_0^\delta(d^\varepsilon) H_1^\delta(d^\varepsilon)(-k'_{str}(1 - d_0)|\partial_z p_0|/2 + d_0 \Sigma_0/2) + (1 - H_1^\delta(d^\varepsilon))[-\Sigma_0/2]_+.$$

The original model is obtained when passing δ to zero [23], obtaining finally

$$\partial_t d_0 = \begin{cases} [\Sigma_0/2]_-, & \text{if } d_0 = 1, \\ -k'_{str}(1 - d_0)|\partial_z p_0|/2 + d_0 \Sigma_0/2, & \text{if } 0 < d_0 < 1, \\ 0, & \text{if } d_0 = 0. \end{cases}$$

5 Discussion and comparison with other biofilm models

The extension from a channel (tube) to a porous medium is done by considering a stack of channels (tubes) of void space and solid material [24], where we denote by ϕ the porosity of the porous medium. Figure 3 shows the core with tubes as void spaces. We assume that all tubes have the same diameter. Therefore, multiplying the upscaled model equations by ϕ, the corresponding core-scale mathematical models are obtained.

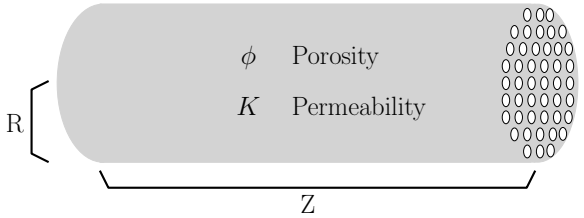

Figure 3: Schematic representation of a porous medium consisting of a stack of thin tubes of void space and solid matrix.

Table 1 shows the core-scale equations of the van Noorden model, the porous medium formed by channels and the porous medium formed by tubes, where $v := \phi q$ is the Darcy velocity. For the details of the upscaling on the thin channel domain, see Appendix A.

Table 1: *Core-Scale Equations for the Three Different Models*

Name	Upscaled equation
Darcy[a]	$v = -\frac{\phi \kappa_c(d)}{\mu}\partial_z p, \quad \partial_z v = 0$
Darcy[b]	$v = -\frac{\phi \kappa_t(d)}{\mu}\partial_z p, \quad \partial_z v = 0$
Darcy[c]	$v = -\frac{2\phi(1-d)^3}{3\mu}\partial_z p, \quad \partial_z v = 0$
Nutrients[a]	$\partial_t(\phi c) + \partial_z\left(cv - \frac{\phi}{P_e}\partial_z c\right) = -d\phi\rho_a R$
Nutrients[b]	$\partial_t(\phi c) + \partial_z\left(cv - \frac{\phi}{P_e}\partial_z c\right) = -(1-(1-d)^2)\phi\rho_a R$
Nutrients[c]	$\partial_t(\phi c) + \partial_z\left(cv - \frac{\phi}{P_e}\partial_z c\right) = -d\phi\rho_a R$
Height[a]	$\partial_t d = \begin{cases} [\Sigma]_-, & \text{if } d = 1, \\ -k_{str}(1-d)\lvert\partial_z p\rvert + d\Sigma, & \text{if } 0 < d < 1, \\ 0, & \text{if } d = 0. \end{cases}$
Height[b]	$\partial_t d = \begin{cases} [\Sigma/2]_-, & \text{if } d = 1, \\ -k_{str}\frac{1-d}{2}\lvert\partial_z p\rvert + d\Sigma/2, & \text{if } 0 < d < 1, \\ 0, & \text{if } d = 0. \end{cases}$
Height[c]	$\partial_t d = \begin{cases} [\Sigma]_-, & \text{if } d = 1, \\ -k_{str}(1-d)\lvert\partial_z p\rvert + d\Sigma, & \text{if } 0 < d < 1, \\ 0, & \text{if } d = 0. \end{cases}$
Bacteria[a,b]	$\partial_t \theta_a = Y_a \mu_n \theta_a \frac{c}{k_n + c} - k_{res}\theta_a - \theta_a \Sigma$
EPS[a,b]	$\partial_t \theta_e = \frac{\rho_a}{\rho_e} Y_e \mu_n \theta_a \frac{c}{k_n + c} - \theta_e \Sigma$
Dead[a,b]	$\partial_t \theta_d = \frac{\rho_a}{\rho_d} k_{res}\theta_a - \theta_d \Sigma$
Reactions[a,b]	$\Sigma := \left(\frac{\rho_a}{\rho_e} Y_e + Y_a\right) R + \left(\frac{\rho_a}{\rho_d} - 1\right) k_{res}\theta_a, \quad R = \mu_n \theta_a \frac{c}{k_n + c}$
Reactions[c]	$\Sigma := Y_a R - k_{res}, \quad R = \mu_n \frac{c}{k_n + c}$

[a]Channel model. [b]Tube model. [c][24].

From Table 1, we observe that for the Darcy flow, the permeability is different for the three models. Figure 4 shows the tube and channel effective permeabilities as a function of the biofilm height for different biofilm permeability values. We observe that the effective permeability decreases as the biofilm height increases and the biofilm permeability decreases.

Figure 5 shows the three different effective permeabilities for a biofilm permeability value of $k = 10^{-1}$. We observe that when there is no biofilm ($d = 0$), the effective permeability in the channel is larger than the effective permeability in the tube, as a result of the upscaling. The other limit case is when the biofilm has clogged the channel ($d = 1$). In this case, for the [24] model, since the biofilm is not permeable, the water flux becomes 0. This is not true in the present model as the biofilm is permeable, reflecting better the realistic situation.

For the nutrients, the difference between [24] and the channel model is on the reaction term, where for [24] the nutrient consumption depends on the biofilm height, while in the channel model depends also in the volume fraction of active bacteria. Comparing the tube and channel model, we observe a different function of the biofilm height, due to the cylindrical geometry. For the biofilm height, the difference between [24] and the channel model is on the Σ term, where for [24] the total sum of reactions accounts for bacterial reproduction and decay, while in the channel model accounts also for EPS. Finally, for the bacterial, EPS, and dead bacterial volume fractions, the model equations are the same for the channel and tube models, while for [24] the active bacterial volume fraction is constant with value 1.

In [24], the authors compared their upscaled model with a well-know macro-scale model by [25], where a mathematical model for an impermeable single-species biofilm including flow, transport and reactions is built. We compare our both derived uspscaled models with a macro-scale model by [6], where a mathematical model for impermeable multi-species biofilm including flow, transport and reactions is built (Table 2).

In Table 2, K is the saturated hydraulic conductivity, θ_B and θ_K the normalized current biodegradation and biobarrier-forming microbial concentrations, ϕ_0 and K_0 the clean surface porosity and initial hydraulic conductivity respectively and η an experimentally determined parameter. In [6], the porosity decreases as the component concentrations increases. In our models, the porosity in the porous medium decreases as the biofilm height increases. However, in [6] the authors do not include the detachment effects. Therefore, the equation for the biofilm height in our models allow the inclusion of the detachment. The permeability in both tube and channel models have different functions as a result of the different geometries and also because of the water flow inside the biofilm. Notice that there is a quartic function of the biofilm height in one of the permeability terms in the porous medium formed by tubes, as proposed in [22] and [17]. For the nutrient transportation, those models, in addition to the [6] model, have the same form with different reaction rates.

We perform numerical simulations considering both effective models (channel and tube) to compare the biofilm height

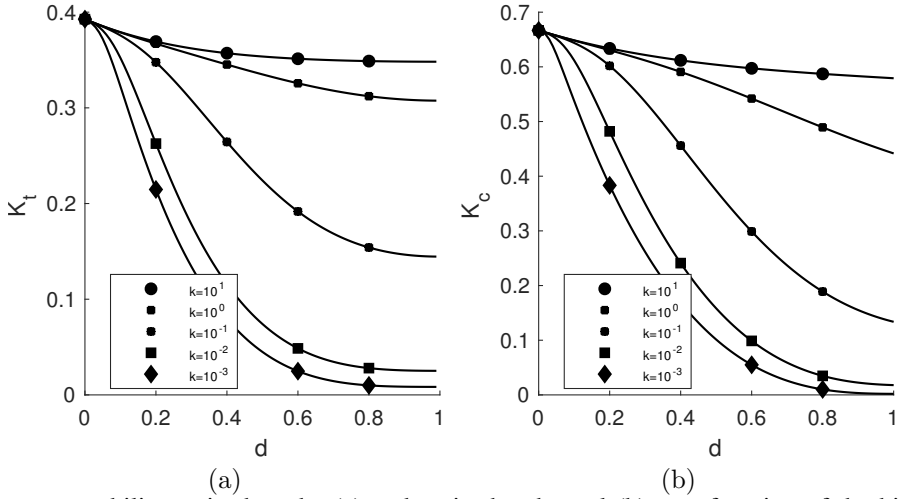

(a) (b)

Figure 4: Effective permeability κ_t in the tube (a) and κ_c in the channel (b) as a function of the biofilm height d for different biofilm permeability values k.

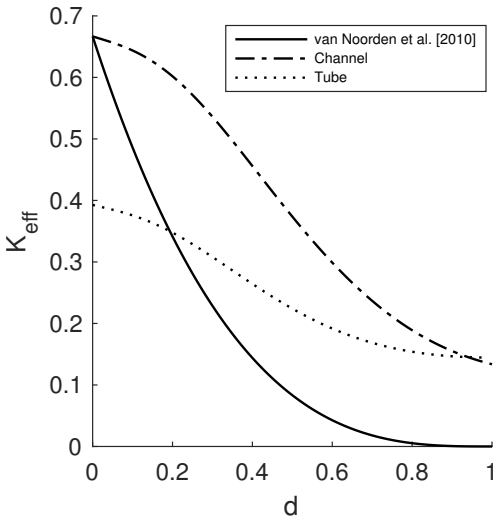

Figure 5: Effective permeabilities of [24], the tube, and the channel models as a function of the biofilm height d for the biofilm permeability value of $k = 10^{-1}$.

over time. We consider two different porous media of length $L = 0.1$ m: the first one has pores formed by thin channels of height $2l = 0.2$ mm and the second ones with tubes of diameter $2\rho = 0.2$ mm. For the inlet boundary, we set $p_i = 2$ Pa. The injected nutrient concentration is $C = 10$ kg/m^3. The porosity Φ is set to 0.4. Recalling that biofilms are mostly composed by water, we set the water volume fraction in the biofilm equal to 90%. In Table 3, the values of parameters for the numerical simulations are presented.

We implement the model equations in the commercial software COMSOL Multiphysics (COMSOL 5.2a, Comsol Inc, Burlington, MA, www.comsol.com). A decoupled finite element algorithm is used to solve the mathematical model equations. Firstly, we solve for the pressure and concentration. Then, we compute the volume fractions and biofilm height. We iterate between both steps until the error E (the difference between successive values of the solution) drops below a given tolerance δ. We perform numerical simulations and we compare the results of the two upscaled mathematical models.

Figure 6 compares the upscaled model with the pore-scale model in the channel for different values of ε, where the percentage of biofilm coverage area over time is plotted. We observe that the percentage of biofilm coverage area in the pore-scale simulations approaches the one computed from the upscaled models as ε gets smaller.

Figure 7 shows the changes over time of biofilm height for both porous media. Initially, the left part ($0 < z < L/2$) has a biofilm height of $d = l/2$ ($d = \rho/2$ for the tubular pores), while the right part ($L > z > L/2$) has a height of $d = l/4$ ($d = \rho/4$ for the tubular pores). We observe that the biofilm height increases faster for the pore channels than in the pore tubes. The explanation of this result is that the right-hand side of the equation for the biofilm height in the tube is half times smaller than the right-hand side of the equation for the biofilm height in the channel which is obtained after upscaling in the two different geometries. For the porous medium formed by channels, we observe that the biofilm keeps growing even though the left part of the pore is clogged. This result cannot be observed using the [24] model because the

Table 2: *Core-Scale Equations for the Model Comparison [6]*

Name	Equation
Darcy	$v = -K\partial_z p, \quad \partial_z v = 0$
Nutrients	$\partial_t c + \partial_z(cv - D\partial_z c) = R$
Porosity	$\phi = \phi_0(1 - \theta_B - \theta_K)$
Permeability	$K = K_0(\phi/\phi_0)^\eta$
Component B	$\partial_t \theta_B = Y_B \mu_B \theta_B \frac{c}{k_B + c} - k_{res}\theta_B$
Component K	$\partial_t \theta_K = Y_K \mu_K \theta_K \frac{c}{k_K + c} - k_{res}\theta_K$
Reactions	$R = -\mu_B \theta_B \frac{c}{k_B + c} - \mu_K \theta_K \frac{c}{k_K + c}$

Table 3: *Model Parameters for the Numerical Studies*

Name	Description	Value
μ	Water dynamic viscosity	10^{-3} Pa·s
ρ_w	Water density	10^3 kg/m^3
μ_n	Maximum growth rate[a]	1.1×10^{-5}/s
k_n	Monod-half velocity[a]	10^{-4} kg/m^3
ρ_e	EPS density[a]	60 kg/m^3
ρ_a	Active bacterial density[a]	60 kg/m^3
ρ_d	Dead bacterial density[a]	60 kg/m^3
k	Biofilm permeability[b]	10^{-9} m^2
D	Nutrient diffusion[c]	1.7×10^{-9} m^2/s
Y_a	Active bacterial growth yield[c]	0.553
Y_e	EPS growth yield[c]	0.447
k_{res}	Bacterial decay rate[c]	3.5×10^{-6}/s
k_{str}	Stress[d]	2.6×10^{-10} m/(s Pa)

[a][2]. [b][7]. [c][10]. [d][14].

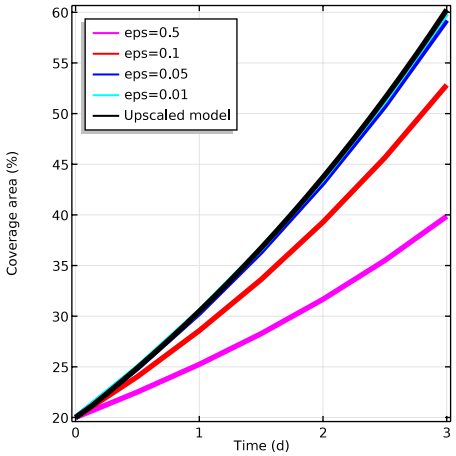

Figure 6: Percentage of biofilm coverage area over time for the upscaled model and for decreasing values of epsilon.

water flux stops once the channel is clogged.

6 Conclusions

In this work, we upscale a mathematical model for permeable biofilm considering a thin channel and tubular pore geometries. The upscaled models differ mainly in the permeability terms which are functions of the biofilm height. After comparison with the [24], it is possible to derive this model as a particular case of the channel model. The derived upscaled models and the [6] model are very similar, the greatest difference being the lack of detachment of biofilm components in the [6] model. The numerical simulations show that the biofilm height increases faster in the porous medium formed by channels than in the one formed by tubes. To validate the core-scale upscaled models, designed laboratory experiments are necessary which is the subject of our future research.

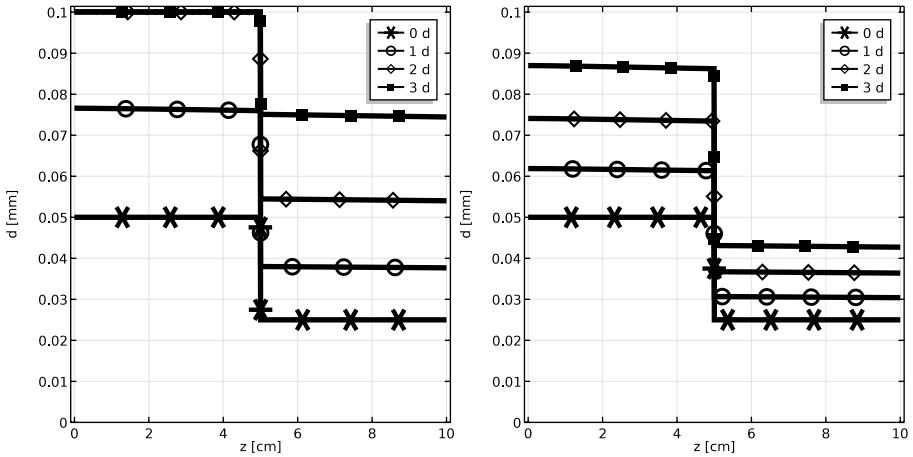

Figure 7: Biofilm height in the porous medium formed by channels (a) and tubes (b).

A Upscaling of the mathematical model in a thin channel

In section 4, we show with details how to obtain the upscaled model equations in a tube. Following the same ideas, in this appendix we show how to upscale the model equations in a channel. We consider a thin channel with height $2l$, thickness w, and length L. When the thickness is much smaller than the height, experiments show that the growing of the biofilm occurs only in the upper and lower walls [15]. Therefore, we can model the biofilm in the thin channel in a two-dimensional domain. Figure 8 shows the different domains, boundaries, and interface in the rectangular geometry.

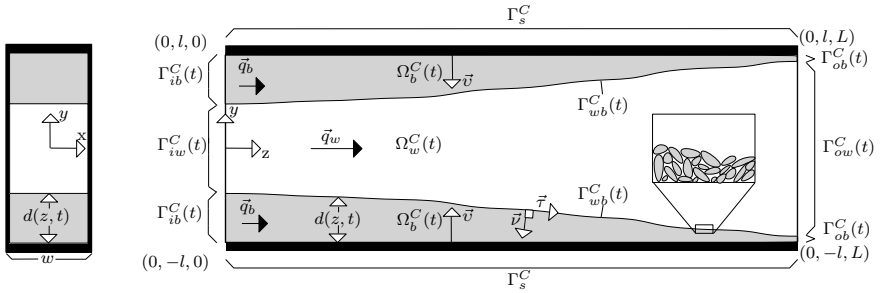

Figure 8: Pore of length L, height $2l$, and thickness w in Cartesian coordinates.

To achieve non-dimensional quantities, we use the reference values defined in section 4 (T, L, Q, U, P, and C). The thin strip is characterized by the ratio of its height to the length $\varepsilon := l/L$.

The two-dimensional space domains for the non-dimensional formulation are given by

$$
\begin{array}{lrcl}
\text{Channel} & \Omega^{C,\varepsilon} & := & [0,1]\times[0,1], \\
\text{Water} & \Omega_w^{C,\varepsilon}(t) & := & \{\vec{x}|\ y\in(-1+d^\varepsilon(z,t),1-d^\varepsilon(z,t)),\ z\in(0,1)\}, \\
\text{Biofilm} & \Omega_b^{C,\varepsilon}(t) & := & \{\vec{x}|\ y\in(-1,-1+d^\varepsilon(z,t))\ \vee\ y\in(1-d^\varepsilon(z,t),1), z\in(0,1)\},
\end{array}
$$

and the boundaries and interface are given by

$$
\begin{aligned}
&\text{Inflow} && \Gamma_i^{C,\varepsilon} &:=\ & [0,1]\times\{0\},\\
&\text{Outflow} && \Gamma_o^{C,\varepsilon} &:=\ & [0,1]\times\{1\},\\
&\text{Water inflow} && \Gamma_{iw}^{C,\varepsilon}(t) &:=\ & \{\vec{x}|\ y\in(-1+d^\varepsilon(z,t),1-d^\varepsilon(z,t)),\ z=0\},\\
&\text{Water outflow} && \Gamma_{ow}^{C,\varepsilon}(t) &:=\ & \{\vec{x}|\ y\in(-1+d^\varepsilon(z,t),1-d^\varepsilon(z,t)),\ z=1\},\\
&\text{Interface} && \Gamma_{wb}^{C,\varepsilon}(t) &:=\ & \{\vec{x}|\ y=\pm(1-d^\varepsilon(z,t)),\ z\in(0,1)\},\\
&\text{Biofilm inflow} && \Gamma_{ib}^{C,\varepsilon}(t) &:=\ & \{\vec{x}|\ y\in(-1,-1+d^\varepsilon(z,t))\ \vee\ y\in(1-d^\varepsilon(z,t),1),\ z=0\},\\
&\text{Biofilm outflow} && \Gamma_{ob}^{C,\varepsilon}(t) &:=\ & \{\vec{x}|\ y\in(-1,-1+d^\varepsilon(z,t))\ \vee\ y\in(1-d^\varepsilon(z,t),1),\ z=1\},\\
&\text{Wall} && \Gamma_s^{C,\varepsilon} &:=\ & \{\pm1\}\times(0,1).
\end{aligned}
$$

The dimensionless system of equations for the water flux is given by

$$
\begin{aligned}
\partial_y q_w^{\varepsilon(y)}+\partial_z q_w^{\varepsilon(z)} &= 0 && \text{in } \Omega_w^{C,\varepsilon}(t), && (61)\\
\mu'(\varepsilon^2\partial_z^2 q_w^{\varepsilon(y)}+\partial_y^2 q_w^{\varepsilon(y)}) &= \varepsilon^{-2}\partial_y p_w^\varepsilon && \text{in } \Omega_w^{C,\varepsilon}(t), && (62)\\
\mu'\varepsilon^2\partial_z^2 q_w^{\varepsilon(z)}+\partial_y^2 q_w^{\varepsilon(z)} &= \partial_z p_w^\varepsilon && \text{in } \Omega_w^{C,\varepsilon}(t), && (63)\\
\partial_y q_b^{\varepsilon(y)}+\partial_z q_b^{\varepsilon(z)} &= 0 && \text{in } \Omega_b^{C,\varepsilon}(t), && (64)\\
\frac{\mu'}{\theta_w}(\varepsilon^2\partial_z^2 q_b^{\varepsilon(y)}+\partial_y^2 q_b^{\varepsilon(y)}) &= \varepsilon^{-2}\partial_y p_b^\varepsilon && \text{in } \Omega_b^{C,\varepsilon}(t), && (65)\\
\frac{\mu'}{\theta_w}(\varepsilon^2\partial_z^2 q_b^{\varepsilon(z)}+\partial_y^2 q_b^{\varepsilon(z)}) &= \partial_z p_b^\varepsilon-\frac{\mu'}{k}(q_b^{\varepsilon(y)},q_b^{\varepsilon(z)}) && \text{in } \Omega_b^{C,\varepsilon}(t), && (66)\\
\nu^{(z)}(\mu'\partial_z q_w^{\varepsilon(z)}-p_w^\varepsilon-\frac{\mu'}{\theta_w}\partial_z q_b^{\varepsilon(z)}+p_b^\varepsilon) &= \varepsilon\nu^{(y)}(\frac{\mu'}{\theta_w}\partial_z q_b^{\varepsilon(y)}-\mu'\partial_z q_w^{\varepsilon(y)}) && \text{at } \Gamma_{wb}^{C,\varepsilon}(t), && (67)\\
\varepsilon\nu^{(y)}(\frac{\mu'}{\theta_w}\partial_y q_b^{\varepsilon(y)}-p_b^\varepsilon-\mu'\partial_y q_w^{\varepsilon(y)}+p_w^\varepsilon) &= \nu^{(z)}(\mu'\partial_y q_w^{\varepsilon(z)}-\frac{\mu'}{\theta_w}\partial_y q_b^{\varepsilon(z)}) && \text{at } \Gamma_{wb}^{C,\varepsilon}(t), && (68)\\
(q_w^{\varepsilon(y)},\ q_w^{\varepsilon(z)}) &= (q_b^{\varepsilon(y)},\ q_b^{\varepsilon(z)}) && \text{at } \Gamma_{wb}^{C,\varepsilon}(t), && (69)\\
(q_b^{\varepsilon(y)},\ q_b^{\varepsilon(z)}) &= (0,\ 0) && \text{at } \Gamma_s^{C,\varepsilon}. && (70)
\end{aligned}
$$

The equations for the nutrients become

$$
\begin{aligned}
\partial_t c_w^\varepsilon-\frac{1}{P_e'}(\varepsilon^{-2}\partial_y^2 c_w^\varepsilon+\partial_z^2 c_w^\varepsilon)+\partial_y(q_w^{\varepsilon(y)}c_w^\varepsilon)+\partial_z(q_w^{\varepsilon(z)}c_w^\varepsilon) &= 0 \quad \text{in } \Omega_w^{C,\varepsilon}(t), && (71)\\
\partial_t(\theta_w c_b^\varepsilon)-\frac{\theta_w}{P_e'}(\varepsilon^{-2}\partial_y^2 c_b^\varepsilon+\partial_z^2 c_b^\varepsilon)+\partial_y(q_b^{\varepsilon(y)}c_b^\varepsilon)+\partial_z(q_b^{\varepsilon(z)}c_b^\varepsilon) &= R_b^\varepsilon \quad \text{in } \Omega_b^{C,\varepsilon}(t), && (72)\\
-\frac{1}{P_e'\varepsilon^2}(\partial_y c_w^\varepsilon-\theta_w\partial_y c_b^\varepsilon)-(c_b^\varepsilon q_b^{\varepsilon(y)}-c_w^\varepsilon q_w^{\varepsilon(y)})+\partial_t d^\varepsilon(\theta_w c_b^\varepsilon-c_w^\varepsilon) & && && \\
+\frac{\partial_z d^\varepsilon}{P_e'}(\partial_z c_w^\varepsilon-\theta_w\partial_z c_b^\varepsilon)+\partial_z d^\varepsilon(c_b^\varepsilon q_b^{\varepsilon(z)}-c_w^\varepsilon q_w^{\varepsilon(z)}) &= 0 \quad \text{at } \Gamma_{wb}^{C,\varepsilon}(t), && (73)\\
\theta_w c_b^\varepsilon &= c_w^\varepsilon \quad \text{at } \Gamma_{wb}^{C,\varepsilon}(t), && (74)\\
\partial_y c_b^\varepsilon &= 0 \quad \text{at } \Gamma_s^{C,\varepsilon}, && (75)
\end{aligned}
$$

where

$$R_b^\varepsilon=-\mu_n'\theta_a^\varepsilon\rho_a'\frac{c_b^\varepsilon}{k_n'+c_b^\varepsilon}.$$

The dimensionless equations for the growth velocity potential are given by

$$\frac{U}{Q}(\partial_y u^{\varepsilon(y)} + \partial_z u^{\varepsilon(z)}) = \Sigma^{\varepsilon} \quad \text{in } \Omega_b^{C,\varepsilon}(t), \tag{76}$$

$$(u^{\varepsilon(y)},\, u^{\varepsilon(z)}) = -(\partial_y \Phi^{\varepsilon}, \varepsilon^2 \partial_z \Phi^{\varepsilon}) \quad \text{in } \Omega_b^{C,\varepsilon}(t), \tag{77}$$

$$\Phi^{\varepsilon} = 0 \quad \text{at } \Gamma_{wb}^{C,\varepsilon}(t), \tag{78}$$

$$\partial_y \Phi^{\varepsilon} = 0 \quad \text{at } \Gamma_s^{C,\varepsilon}, \tag{79}$$

where

$$\Sigma^{\varepsilon} := \left(\frac{\rho_a^{'}}{\rho_e^{'}} Y_e + Y_a\right) \mu_n^{'} \theta_a^{\varepsilon} \frac{c}{k_n^{'} + c} + \left(\frac{\rho_a^{'}}{\rho_d^{'}} - 1\right) k_{res}^{'} \theta_a^{\varepsilon}.$$

The equations for the biomass components become

$$\partial_t \theta_e^{\varepsilon} + \frac{U}{Q}(u^{\varepsilon(y)} \partial_z \theta_e^{\varepsilon} + u^{\varepsilon(z)} \partial_y \theta_e^{\varepsilon}) = Y_e \mu_n^{'} \theta_a^{\varepsilon} \frac{\rho_a^{'}}{\rho_e^{'}} \frac{c_b^{\varepsilon}}{k_n^{'} + c_b^{\varepsilon}} - \theta_e^{\varepsilon} \Sigma^{\varepsilon} \quad \text{in } \Omega_b^{C,\varepsilon}(t), \tag{80}$$

$$\partial_t \theta_a^{\varepsilon} + \frac{U}{Q}(u^{\varepsilon(y)} \partial_z \theta_a^{\varepsilon} + u^{\varepsilon(z)} \partial_y \theta_a^{\varepsilon}) = Y_a \mu_n^{'} \theta_a^{\varepsilon} \frac{c_b^{\varepsilon}}{k_n^{'} + c_b^{\varepsilon}} - k_{res}^{'} \theta_a^{\varepsilon} - \theta_a^{\varepsilon} \Sigma^{\varepsilon} \quad \text{in } \Omega_b^{C,\varepsilon}(t), \tag{81}$$

$$\partial_t \theta_d^{\varepsilon} + \frac{U}{Q}(u^{\varepsilon(y)} \partial_z \theta_d^{\varepsilon} + u^{\varepsilon(z)} \partial_y \theta_d^{\varepsilon}) = k_{res}^{'} \frac{\rho_a^{'}}{\rho_d^{'}} \theta_a^{\varepsilon} - \theta_d^{\varepsilon} \Sigma^{\varepsilon} \quad \text{in } \Omega_b^{C,\varepsilon}(t), \tag{82}$$

$$-\partial_y \theta_i + \varepsilon \partial_z d^{\varepsilon} \partial_z \theta_i = 0 \quad i \in \{e,a,d\} \quad \text{at } \Gamma_{wb}^{C,\varepsilon}(t), \tag{83}$$

$$\partial_y \theta_i = 0 \quad i \in \{e,a,d\} \quad \text{at } \Gamma_s^{C,\varepsilon}. \tag{84}$$

For the biofilm height we have

$$\partial_t d^{\varepsilon} = \begin{cases} [-\frac{U}{Q}(-u^{\varepsilon(y)} + \partial_z d^{\varepsilon} u^{\varepsilon(z)})]_+, & \text{if } d = 1, \\ -\sqrt{1 + (\varepsilon \partial_z d^{\varepsilon})^2}\, \varepsilon k_{str}^{'} S^{'} - \frac{U}{Q}(-u^{\varepsilon(y)} + \partial_z d^{\varepsilon} u^{\varepsilon(z)}), & \text{if } 0 < d < 1, \text{ at } \Gamma_{wb}^{C,\varepsilon}(t), \\ 0, & \text{if } d = 0, \end{cases} \tag{85}$$

where

$$S^{'} = ||(I - \nu^{\varepsilon} \nu^{\varepsilon T}) \mu^{'} M^{'} \nu^{\varepsilon}||, \tag{86}$$

and

$$M^{'} = \begin{pmatrix} \partial_y q_w^{\varepsilon(y)} & \varepsilon \partial_z q_w^{\varepsilon(y)} \\ \varepsilon^{-1} \partial_y q_w^{\varepsilon(z)} & \partial_z q_w^{\varepsilon(z)} \end{pmatrix}. \tag{87}$$

We define the average water flow as the following integral

$$\bar{q}(z,t) = \bar{q}_w(z,t) + \bar{q}_b(z,t) = \int_{-(1-d_0)}^{1-d_0} q_{w,0}^{(z)} dy + \int_{-1}^{-(1-d_0)} q_{b,0}^{(z)} dy + \int_{1-d_0}^{1} q_{b,0}^{(z)} dy. \tag{88}$$

We define the following space regions in the channel

$$\begin{aligned} \Xi_u^{'} &= \{\vec{x} |\, 1 - d^{\varepsilon} \le y \le 1 \,\wedge\, z_1 \le z \le z_1 + \delta z\}, \\ \Xi_m^{'} &= \{\vec{x} |\, |y| \le 1 - d^{\varepsilon} \,\wedge\, z_1 \le z \le z_1 + \delta z\}, \\ \Xi_l^{'} &= \{\vec{x} |\, -1 \le y \le -(1 - d^{\varepsilon}) \,\wedge\, z_1 \le z \le z_1 + \delta z\}. \end{aligned}$$

Integrating (61) and (64) over the previous regions and using the Gauss Theorem yield

$$
\begin{aligned}
0 = \quad & \int_{\Xi_u} \nabla\cdot\vec{q}_b^{\,\varepsilon} dV + \int_{\Xi_m} \nabla\cdot\vec{q}_w^{\,\varepsilon} dV + \int_{\Xi_l} \nabla\cdot\vec{q}_b^{\,\varepsilon} dV \\
= \quad & 2\int_{z_1}^{z_1+\delta_z} \vec{q}_w^{\,\varepsilon}\cdot\vec{\nu}\big|_{y=1-d^\varepsilon} dz + \int_{-(1-d_0)}^{1-d_0} (q_w^{\varepsilon(z)}\big|_{z=z_1+\delta_z} - q_w^{\varepsilon(z)}\big|_{z=z_1}) dy \\
& - \int_{z_1}^{z_1+\delta_z} (\vec{q}_b^{\,\varepsilon}\cdot\vec{\nu}\big|_{y=-(1-d^\varepsilon)} + \vec{q}_b^{\,\varepsilon}\cdot\vec{\nu}\big|_{y=-1}) dz + \int_{-1}^{-(1-d^\varepsilon)} (q_b^{\varepsilon(z)}\big|_{z=z_1+\delta_z} - q_b^{\varepsilon(z)}\big|_{z=z_1}) dy \\
& - \int_{z_1}^{z_1+\delta_z} (\vec{q}_b^{\,\varepsilon}\cdot\vec{\nu}\big|_{y=1} + \vec{q}_b^{\,\varepsilon}\cdot\vec{\nu}\big|_{y=1-d}) dz + \int_{1-d^\varepsilon}^{1} (q_b^{\varepsilon(z)}\big|_{z=z_1+\delta_z} - q_b^{\varepsilon(z)}\big|_{z=z_1}) dy.
\end{aligned}
$$

Recalling the no-slip condition for the water flux on the wall (70) and the continuity of fluxes at the interface (69), the previous equation becomes

$$
\begin{aligned}
\int_{-(1-d_0)}^{1-d_0} (q_w^{\varepsilon(z)}\big|_{z=z_1+\delta_z} - q_w^{\varepsilon(z)}\big|_{z=z_1}) dy + \int_{-1}^{-(1-d^\varepsilon)} (q_b^{\varepsilon(z)}\big|_{z=z_1+\delta_z} - q_b^{\varepsilon(z)}\big|_{z=z_1}) dy \\
+ \int_{1-d^\varepsilon}^{1} (q_b^{\varepsilon(z)}\big|_{z=z_1+\delta_z} - q_b^{\varepsilon(z)}\big|_{z=z_1}) dy \qquad = 0.
\end{aligned}
$$

Dividing the previous equation by δ_z and letting δ_z approach zero, we obtain for the lowest-order terms in ε

$$
\partial_z \bar{q} = \partial_z \bar{q}_w(z,t) + \partial_z \bar{q}_b(z,t) = 0,
$$

where we have used the definition of the average water flow (88).
The lowest order terms in the Stokes model (61-63) leads to

$$
\partial_y q_{w,0}^{(y)} + \partial_z q_{w,0}^{(z)} = 0, \qquad \partial_y p_{w,0} = 0, \qquad \mu\,\partial_y^2 q_{w,0}^{(z)} = \partial_z p_{w,0}. \tag{89}
$$

From (89b), we conclude that $p_{w,0}$ does not depend on the y coordinate. Analogous, for the Brinkman model (64-66), the lower-order terms in ε give

$$
\partial_y q_{b,0}^{(y)} + \partial_z q_{b,0}^{(z)} = 0, \qquad \partial_y p_{b,0} = 0, \qquad \frac{\mu}{\theta_w}\partial_y^2 q_{b,0}^{(z)} - \frac{\mu}{k} q_{b,0}^{(z)} = \partial_z p_{b,0}. \tag{90}
$$

From (90b), we conclude that $p_{b,0}$ does not depend on the y coordinate, and from (68) we conclude that $p_{w,0}(z,t) = p_{b,0}(z,t) := p_0(z,t)$. Integrating twice (89) and (90) with respect to y and using the symmetry, interface, and boundary conditions

$$
q_{w,0}^{(z)} = \left(\frac{y^2}{2} + V\right)\frac{\partial_z p_0}{\mu}, \tag{91}
$$

$$
q_{b,0}^{(z)} = \left(We^{y\sqrt{\theta_w/k}} + Xe^{-y\sqrt{\theta_w/k}} - k\right)\frac{\partial_z p_0}{\mu}, \tag{92}
$$

where the coefficients are given by

$$
\begin{aligned}
V = \quad & -\frac{(\frac{h^2}{2}+k)(e^{-d_0\sqrt{\theta_w/k}} + e^{d_0\sqrt{\theta_w/k}}) + \sqrt{k\theta_w}h(e^{-d_0\sqrt{\theta_w/k}} - e^{d_0\sqrt{\theta_w/k}}) - 2k}{e^{-d_0\sqrt{\theta_w/k}} + e^{d_0\sqrt{\theta_w/k}}}, \\
W = \quad & \frac{k e^{-h\sqrt{\theta_w/k}) + \sqrt{k\theta_w}he^{\sqrt{\theta_w/k}}}}{e^{-d_0\sqrt{\theta_w/k}} + e^{d_0\sqrt{\theta_w/k}}}, \\
X = \quad & \frac{k e^{h\sqrt{\theta_w/k}) - \sqrt{k\theta_w}he^{-\sqrt{\theta_w/k}}}}{e^{-d_0\sqrt{\theta_w/k}} + e^{d_0\sqrt{\theta_w/k}}}, \\
h = \quad & -1 + d_0.
\end{aligned}
$$

To obtain the average water flow defined in (88), we integrate (91) and (92) as follows

$$
\begin{aligned}
\bar{q} = \quad & \frac{\partial_z p_0}{\mu_,}\left(\int_{-(1-d_0)}^{1-d_0}\left(\frac{y^2}{2}+V\right)dy + 2\int_{-1}^{-(1-d_0)}\left(We^{y\sqrt{\theta_w/k_,}} + Xe^{-y\sqrt{\theta_w/k_,}} - k_,\right)dy\right) \\
= \quad & \left(\frac{(1-d_0)^3+6V(1-d_0)}{3} + 2\left(\sqrt{\frac{k_,}{\theta_w}}We^{-\sqrt{\theta_w/k_,}}(e^{d_0\sqrt{\theta_w/k_,}}-1)\right.\right. \\
& \left.\left. -\sqrt{\frac{k_,}{\theta_w}}Xe^{\sqrt{\theta_w/k_,}}(e^{-d_0\sqrt{\theta_w/k_,}}-1) - k_,d_0\right)\right)\frac{\partial_z p_0}{\mu_,} \\
= \quad & -\frac{\kappa_c(d_0)}{\mu_,}\partial_z p_0.
\end{aligned}
$$

This is the Darcy law

$$
\bar{q} = -\frac{\kappa_c(d_0)}{\mu_,}\partial_z p_0,
$$

where $\kappa_c(d_0)$ is the effective permeability given by

$$
\begin{aligned}
\kappa_c(d_0) = \quad & -\left(\frac{(1-d_0)^3+6V(1-d_0)}{3} + 2\left(\sqrt{\frac{k_,}{\theta_w}}We^{-\sqrt{\theta_w/k_,}}(e^{d_0\sqrt{\theta_w/k_,}}-1)\right.\right. \\
& \left.\left. -\sqrt{\frac{k_,}{\theta_w}}Xe^{\sqrt{\theta_w/k_,}}(e^{-d_0\sqrt{\theta_w/k_,}}-1) - k_,d_0\right)\right).
\end{aligned}
$$

The growth velocity potential equations (76) and (77) for the lower-order terms in ε are

$$
\frac{U}{Q}(\partial_y u_0^{(y)} + \partial_z u_0^{(z)}) = \Sigma_0, \qquad u_0^{(y)} = -\partial_y \Phi_{b,0}, \qquad u_0^{(z)} = 0, \tag{93}
$$

where the conditions at the interface (78) becomes $\Phi_{b,0} = 0$ and wall (79) becomes $\partial_y \Phi_{b,0} = 0$.
In dimensionless form, the volume fraction equations (80-82) are

$$
\partial_t \theta_i^\varepsilon + \frac{U}{Q}(u^{\varepsilon(y)}\partial_y \theta_i^\varepsilon + u^{\varepsilon(z)}\partial_z \theta_i^\varepsilon) = R_i^\varepsilon - \theta_i^\varepsilon \Sigma^\varepsilon, \tag{94}
$$

with $i = \{e,a,d\}$. We focus on biofilms where the biomass components change slightly along the y direction, resulting in the approximation $\theta_{i,0}(y,z,t) = \theta_{i,0}(z,t)$. Using (93c), the lower-order terms in (94) are

$$
\partial_t \theta_{i,0} = R_{i,0} - \theta_{i,0}\Sigma_0. \tag{95}
$$

Integrating (93a) over y and using the boundary conditions (78)-(79) one gets

$$
u_0^{(y)} = \frac{Q}{U}\Sigma_0(y+1). \tag{96}
$$

For the nutrients, integrating (71) and (72) y yields

$$
\begin{aligned}
& \int_{-(1-d^\varepsilon)}^{1-d^\varepsilon}\left(\partial_t c_w^\varepsilon - \frac{1}{P_e}(\varepsilon^{-2}\partial_y^2 c_w^\varepsilon + \partial_z^2 c_w^\varepsilon) + \partial_y(q_w^{\varepsilon(y)}c_w^\varepsilon) + \partial_z(q_w^{\varepsilon(z)}c_w^\varepsilon)\right)dy \quad = 0, \\
& 2\int_{-1}^{-(1-d^\varepsilon)}\left(\partial_t(\theta_w c_b^\varepsilon) - \frac{\theta_w}{P_e}(\varepsilon^{-2}\partial_y^2 c_b^\varepsilon + \partial_z^2 c_b^\varepsilon) + \partial_y(q_b^{\varepsilon(y)}c_b^\varepsilon) + \partial_z(q_b^{\varepsilon(z)}c_b^\varepsilon)\right. \\
& \qquad \left. + \mu_{n,}\theta_a^\varepsilon \rho_{a,}\frac{c_b^\varepsilon}{k_{n,}+c_b^\varepsilon}\right)dy \quad = 0.
\end{aligned}
$$

Interchanging the integration and the differentiation operators, these equations become

$$\partial_t\left(\int_{-(1-d^\varepsilon)}^{1-d^\varepsilon} c_w^\varepsilon dy\right)+2\partial_t d^\varepsilon c_w^\varepsilon\big|_{y=-(1-d^\varepsilon)}-\partial_z\left(\int_{-(1-d^\varepsilon)}^{1-d^\varepsilon}\left(\frac{1}{P_e'}\partial_z c_w^\varepsilon-q_w^{\varepsilon(z)}c_w^\varepsilon\right)dy\right)$$
$$-2\partial_z d^\varepsilon\left(\frac{1}{P_e'}\partial_z c_w^\varepsilon-q_w^{\varepsilon(z)}c_w^\varepsilon\right)\big|_{y=-(1-d^\varepsilon)}+2\left(\frac{1}{\varepsilon^2 P_e'}\partial_y c_w^\varepsilon-q_w^{\varepsilon(y)}c_w^\varepsilon\right)\big|_{y=-(1-d^\varepsilon)}=0, \tag{97}$$
$$2\partial_t\left(\int_{-1}^{-(1-d^\varepsilon)}\theta_w c_b^\varepsilon dy\right)-2\partial_t d^\varepsilon\theta_w c_b^\varepsilon\big|_{y=-(1-d^\varepsilon)}$$
$$-2\partial_z\left(\int_{-1}^{-(1-d^\varepsilon)}\left(\frac{\theta_w}{P_e'}\partial_z c_b^\varepsilon-q_b^{\varepsilon(z)}c_b^\varepsilon\right)dy\right)+2\partial_z d^\varepsilon\left(\frac{\theta_w}{P_e'}\partial_z c_b^\varepsilon-q_b^{\varepsilon(z)}c_b^\varepsilon\right)\big|_{y=-(1-d^\varepsilon)} \tag{98}$$
$$-2\left(\frac{\theta_w}{\varepsilon^2 P_e'}\partial_y c_b^\varepsilon-q_b^{\varepsilon(y)}c_b^\varepsilon\right)\big|_{y=-(1-d^\varepsilon)}+2\mu_n'\rho_a'\int_{-1}^{-(1-d^\varepsilon)}\theta_a^\varepsilon\frac{c_b^\varepsilon}{k_n'+c_b^\varepsilon}dy=0.$$

Next, the lower order terms in the equations for the conservation of nutrients (71)-(72) are

$$\partial_y^2 c_{w,0}=0,\qquad \partial_y^2 c_{b,0}=0.$$

The interface coupling condition (73) becomes $\theta_w\partial_y c_{b,0}=\partial_y c_{w,0}$ and (74) becomes $\theta_w c_{b,0}=c_{w,0}$, while the boundary condition on the wall (75) becomes $\partial_y c_{b,0}=0$. The symmetry in y implies that both nutrient concentrations do not depend on y, resulting in $c_{w,0}(z,t)=\theta_w c_{b,0}(z,t):=c_0(z,t)$. Using the aforementioned results, both equations (97) and (98) can be written as

$$\partial_t(c_0(2-2d_0))+2\partial_t d_0 c_0\big|_{y=-(1-d_0)}-\frac{2-2d_0}{P_e'}\partial_z^2 c_0+c_0\int_{-(1-d_0)}^{1-d_0}q_{w,0}^{(z)}dy$$
$$-2\partial_z d_0\left(\frac{1}{P_e'}\partial_z c_0-q_w^{(z)}c_0\right)\big|_{y=-(1-d_0)}+2\left(\frac{1}{\varepsilon^2 P_e'}\partial_y c_0-q_{w,0}^{(y)}c_0\right)\big|_{y=-(1-d_0)}=0,$$
$$\partial_t(2d_0c_0)-2\partial_t d_0c_0\big|_{y=-(1-d_0)}-2d_0\frac{1}{P_e'}\partial_z^2 c_0+c_0\int_{-1}^{-(1-d^\varepsilon)}q_{b,0}^{(z)}dy$$
$$+2\partial_z d_0\left(\frac{1}{P_e'}\partial_z c_0-q_{b,0}^{(z)}c_0\right)\big|_{y=-(1-d^\varepsilon)}-2\left(\frac{1}{\varepsilon^2 P_e'}\partial_y c_0-q_{b,0}^{(y)}c_0\right)\big|_{y=-(1-d^\varepsilon)}$$
$$+2d_0\mu_n'\rho_a'\theta_{a,0}\frac{c_0}{k_n'+c_0}=0.$$

Then, adding both equations and using the interface condition (73), we finally obtain

$$\partial_t c_0+\partial_z\left(c_0\bar{q}-\frac{1}{P_e'}\partial_z c_0\right)=-d_0\mu_n'\theta_{a,0}\rho_a'\frac{c_0}{k_n'+c_0}.$$

We focus on the water-biofilm interface (85):

$$\partial_t d^\varepsilon=\begin{cases}[-\frac{U}{Q}(-u^{\varepsilon(y)}+\partial_z d^\varepsilon u^{\varepsilon(z)})]_+, & \text{if } d=1,\\ -\sqrt{1+(\varepsilon\partial_z d^\varepsilon)^2}\varepsilon k_{str}'\mu'||(I-\nu^\varepsilon\nu^{\varepsilon T})M'\nu^\varepsilon||-\frac{U}{Q}(-u^{\varepsilon(y)}+\partial_z d^\varepsilon u^{\varepsilon(z)}), & \text{if } 0<d<1,\\ 0, & \text{if } d=0.\end{cases}$$

Using the set-valued Heaviside graphs (56), we can write the previous equations as

$$\partial_t d^\varepsilon\in H_0(d^\varepsilon)H_1(d^\varepsilon))\left(-\sqrt{1+(\varepsilon\partial_z d^\varepsilon)^2}\varepsilon k_{str}'\mu'||(I-\nu^\varepsilon\nu^{\varepsilon T})M'\nu^\varepsilon||\right. \tag{99}$$
$$\left.-\frac{U}{Q}(-u^{\varepsilon(y)}+\partial_z d^\varepsilon u^{\varepsilon(z)})\right)+(1-H_1(d^\varepsilon))[-\frac{U}{Q}(-u^{\varepsilon(y)}+\partial_z d^\varepsilon u^{\varepsilon(z)})]_+.$$

Using the regularized Heaviside functions (58), we can write (99) as

$$\partial_t d^\varepsilon=H_0^\delta(d^\varepsilon)H_1^\delta(d^\varepsilon))\left(-\sqrt{1+(\varepsilon\partial_z d^\varepsilon)^2}\varepsilon k_{str}'\mu'||(I-\nu^\varepsilon\nu^{\varepsilon T})M'\nu^\varepsilon||\right.$$
$$\left.-\frac{U}{Q}(-u^{\varepsilon(y)}+\partial_z d^\varepsilon u^{\varepsilon(z)})\right)+(1-H_1^\delta(d^\varepsilon))[-\frac{U}{Q}(-u^{\varepsilon(y)}+\partial_z d^\varepsilon u^{\varepsilon(z)})]_+.$$

Using (86-87,91,93a,96), for the lower-order terms in ε we have

$$\partial_t d^\varepsilon = H_0^\delta(d^\varepsilon)H_1^\delta(d^\varepsilon))(-k_{str}^{'}(1-d_0)|\partial_z p_0| + d_0\Sigma_0) + (1-H_1^\delta(d^\varepsilon))[-\Sigma_0]_+.$$

Letting δ go to zero in order to return to the nonregularized formulation, we get

$$\partial_t d_0 = \begin{cases} [\Sigma_0]_- & \text{if } d_0 = 1, \\ -k_{str}^{'}(1-d_0)|\partial_z p_0| + d_0\Sigma_0, & \text{if } 0 < d_0 < 1, \\ 0, & \text{if } d = 0. \end{cases}$$

Acknowledgements The work of D. Landa-Marbán, K. Kumar, Gunhild Bødtker, and F. A. Radu was partially supported by GOE.IP and the Research Council of Norway through the projects IMMENS no. 255426 and CHI no. 255510. I. S. Pop was supported by the Research Foundation-Flanders (FWO) through the Odysseus programme (project G0G1316N) and by Equinor through the Akademia grant. The authors would like to thank Brenna Connolly for improving the writing of the manuscript.

References

[1] Aggarwal, S., Stewart, P. S., Hozalski, R. M.: Biofilm cohesive strength as a basis for biofilm recalcitrance: Are bacterial biofilms overdesigned? Microbiology Insights. (2015). doi:10.4137/MBI.S31444

[2] Alpkvist, E., Klapper, I.: A multidimensional multispecies continuum model for heterogeneous biofilm development. Bulletin of Mathematical Biology. (2007). doi:10.1.1/jpb001

[3] Bott, T. R., Miller, P. C.: Mechanisms of biofilm formation on aluminium tubes. Journal of Chemical Technology and Biotechnology. Biotechnology. (1983). doi:10.1002/jctb.280330307

[4] Bringedal, C., Berre, I., Pop, I. S., Radu, F. A.: A model for non-isothermal flow and mineral precipitation and dissolution in a thin strip. Journal of Computational and Applied Mathematics. (2015). doi:10.1016/j.cam.2014.12.009

[5] Capdeville, B., Rols, J. L.: Introduction to biofilms in water and wastewater treatment. In: Melo, L. F., Bott, T. R., Fletcher, M., Capdeville, B. (eds.). Biofilms – Science and Technology. NATO ASI Series (Series E: Applied Sciences) (1992). **223**, 13–20. Dordrecht, Springer.

[6] Chen-Charpentier, B. M., Dimitrov, D. T., Kojouharov, H. V.: Numerical simulation of multi-species biofilms in porous media for different kinetics. Mathematics and Computers in Simulation. (2009). doi:10.1016/j.matcom.2007.03.002

[7] Deng, W., Bayani Cardenas, M., Kirk, M. F., Altman, S. J., Bennett, P. C.: Effect of permeable biofilm on micro–and macro–scale flow and transport in bioclogged pores. Environmental Science and Technology. (2013). doi:10.1021/es402596v

[8] Donlan, R. M.: Biofilms: Microbial life on surfaces. Emerging Infectious Diseases. (2002). doi:10.3201/eid0809.020063

[9] Flemming, H. C., Wingender, J.: The biofilm matrix. Nature Reviews Microbiology. (2010). doi:10.1038/nrmicro2415

[10] Duddu, R., Chopp, D. L., Moran, B.: A two-dimensional continuum model of biofilm growth incorporating fluid flow and shear stress based detachment. Biotechnology and Bioengineering. (2009). doi:10.1002/bit.22233

[11] Helmig, R., Braun, C., Manthey, S.: Upscaling of two-phase flow processes in heterogeneous porous media: Determination of constitutive relationships. Acta Universitatis Carolinae - Geologica. (2002). **46** (277), 28–36.

[12] Kokare, C. R., Chakraborty, S., Khopade, A. N., Mahadik, K. R.: Biofilm: Importance and applications. Indian Journal of Biotechnology. (2009), **8**, 159–168.

[13] Kumar, K., van Noorden, T. L., Pop, I. S.: Upscaling of reactive flows in domains with moving oscillating boundaries. Discrete & Continuous Dynamical Systems - S. (2014). doi:10.3934/dcdss.2014.7.95

[14] Landa-Marbán, D., Liu, N., Pop, I. S., Kumar, K., Pettersson, P., Bødtker, G., Skauge, T., Radu, F. A.: A pore-scale model for permeable biofilm: Numerical simulations and laboratory experiments. Under revision.

[15] Liu, N., Skauge, T., Landa-Marbán, D., Hovland, B., Thorbjørnsen, B., Radu, F. A., Vik, B. F., Baumann, T., Bødtker, G.: Microfluidic study of effects of flowrate and nutrient concentration on biofilm accumulation and adhesive strength in a microchannel. Under revision.

[16] Miranda, A. F., Ramkumar, N., Andriotis, C., Höltkemeier, T., Yasmin, A., Rochfort, S., Wlodkowic, D., Morrison, P., Roddick, F., Spangenberg, G., Lal, B., Subudhi, S., Mouradov, A.: Applications of microalgal biofilms for wastewater treatment and bioenergy production. Biotechnology for Biofuels. (2017). doi:10.1186/s13068-017-0798-9

[17] Mostafa, M., van Geel, P.: Conceptual models and simulations for biological clogging in unsaturated soils. Vadose Zone Journal. (2007). doi:10.2136/vzj2006.0033

[18] Olver, F. W. J.: Bessel funtions of integer order. In: Abramowitz, M., Stegun, I.A. (eds.).Handbook of mathematical functions: With formulas, graphs, and mathematical tables. Dover Books on Mathematics. (2012). Dover Publications. 355–434. Mineola, NY.

[19] Peszynska, M., Trykozko, A., Iltis, G., Steffen, S., Wildenschild, D.: Biofilm growth in porous media: Experiments, computational modeling at the porescale, and upscaling. Advances in Water Resources. (2016). doi:10.1016/j.advwatres.2015.07.008

[20] Raiders, R. A., Knapp, R. M., McInerney, M. J.: Microbial selective plugging and enhanced oil recovery. Journal of Industrial Microbiology. (1989). doi:10.1007/BF01574079

[21] Schulz, R., Knabner, P.: Derivation and analysis of an effective model for biofilm growth in evolving porous media. Mathematical Methods in the Applied Sciences. (2016). doi:10.1002/mma.4211

[22] Suchomel, B. J., Chen, B. M., Allen, M. B.: Macroscale properties of porous media from a network model of biofilm processes. Transport in Porous Media. (1998). doi:10.1023/A:1006506104835

[23] van Duijn, C. J., Pop, I. S.: Crystal dissolution and precipitation in porous media: Pore scale analysis. Journal für die reine und angewandte Mathematik (Crelles Journal). (2004). doi:10.1515/crll.2004.2004.577.171

[24] van Noorden, T. L., Pop, I. S., Ebigbo, A., Helmig, R.: An upscaled model for biofilm growth in a thin strip. Water Resources Research. (2010). doi:10.1029/2009WR008217

[25] Taylor, S. W., Jaffé, P. R.: Substrate and biomass transport in a porous medium. Water Resources Research. (1990). doi:10.1029/WR026i009p02181

[26] Vu, B., Chen, M. and Crawford, R. J. and Ivanova, E. P.: Bacterial extracellular polysaccharides involved in biofilm formation. Molecules. (2009). doi:10.3390/molecules14072535

UHasselt Computational Mathematics Preprint Series

2018

UP-18-09 *David Landa-Marbán, Gunhild Bødtker, Kundan Kumar, Iuliu Sorin Pop, Florin Adrian Radu*, **An upscaled model for permeable biofilm in a thin channel and tube**, 2018

UP-18-08 *Vo Anh Khoa, Le Thi Phuong Ngoc, Nguyen Thanh Long*, **Existence, blow-up and exponential decay of solutions for a porous-elastic system with damping and source terms**, 2018

UP-18-07 *Vo Anh Khoa, Tran The Hung, Daniel Lesnic*, **Uniqueness result for an age-dependent reaction-diffusion problem**, 2018

UP-18-06 *Koondanibha Mitra, Iuliu Sorin Pop*, **A modified L-Scheme to solve nonlinear diffusion problems**, 2018

UP-18-05 *David Landa-Marban, Na Liu, Iuliu Sorin Pop, Kundan Kumar, Per Pettersson, Gunhild Bodtker, Tormod Skauge, Florin A. Radu*, **A pore-scale model for permeable biofilm: numerical simulations and laboratory experiments**, 2018

UP-18-04 *Florian List, Kundan Kumar, Iuliu Sorin Pop and Florin A. Radu*, **Rigorous upscaling of unsaturated flow in fractured porous media**, 2018

UP-18-03 *Koondanibha Mitra, Hans van Duijn*, **Wetting fronts in unsaturated porous media: the combined case of hysteresis and dynamic capillary**, 2018

UP-18-02 *Xiulei Cao, Koondanibha Mitra*, **Error estimates for a mixed finite element discretization of a two-phase porous media flow model with dynamic capillarity**, 2018

UP-18-01 *Klaus Kaiser, Jonas Zeifang, Jochen Schütz, Andrea Beck and Claus-Dieter Munz*, **Comparison of different splitting techniques for the isentropic Euler equations**, 2018

2017

UP-17-12 *Carina Bringedal, Tor Eldevik, Øystein Skagseth and Michael A. Spall*, **Structure and forcing of observed exchanges across the Greenland-Scotland Ridge**, 2017

UP-17-11 *Jakub Wiktor Both, Kundan Kumar, Jan Martin Nordbotten, Iuliu Sorin Pop and Florin Adrian Radu*, **Linear iterative schemes for doubly degenerate parabolic equations**, 2017

UP-17-10 *Carina Bringedal and Kundan Kumar*, **Effective behavior near clogging in upscaled equations for non-isothermal reactive porous media flow**, 2017

UP-17-09 *Alexander Jaust, Balthasar Reuter, Vadym Aizinger, Jochen Schütz and Peter Knabner*, **FESTUNG: A MATLAB / GNU Octave toolbox for the discontinuous Galerkin method. Part III: Hybridized discontinuous Galerkin (HDG) formulation**, 2017

UP-17-08 *David Seus, Koondanibha Mitra, Iuliu Sorin Pop, Florin Adrian Radu and Christian Rohde*, **A linear domain decomposition method for partially saturated flow in porous media**, 2017

UP-17-07 *Klaus Kaiser and Jochen Schütz*, **Asymptotic Error Analysis of an IMEX Runge-Kutta method**, 2017

UP-17-06 *Hans van Duijn, Koondanibha Mitra and Iuliu Sorin Pop*, **Travelling wave solutions for the Richards equation incorporating non-equilibrium effects in the capillarity pressure**, 2017

UP-17-05 *Hans van Duijn and Koondanibha Mitra*, **Hysteresis and Horizontal Redistribution in Porous Media**, 2017

UP-17-04 *Jonas Zeifang, Klaus Kaiser, Andrea Beck, Jochen Schütz and Claus-Dieter Munz*, **Efficient high-order discontinuous Galerkin computations of low Mach number flows**, 2017

UP-17-03 *Maikel Bosschaert, Sebastiaan Janssens and Yuri Kuznetsov*, **Switching to nonhyperbolic cycles from codim-2 bifurcations of equilibria in DDEs**, 2017

UP-17-02 *Jochen Schütz, David C. Seal and Alexander Jaust*, **Implicit multiderivative collocation solvers for linear partial differential equations with discontinuous Galerkin spatial discretizations**, 2017

UP-17-01 *Alexander Jaust and Jochen Schütz*, **General linear methods for time-dependent PDEs**, 2017

2016

UP-16-06 *Klaus Kaiser and Jochen Schütz*, **A high-order method for weakly compressible flows**, 2016

UP-16-05 *Stefan Karpinski, Iuliu Sorin Pop, Florin A. Radu*, **A hierarchical scale separation approach for the hybridized discontinuous Galerkin method**, 2016

UP-16-04 *Florin A. Radu, Kundan Kumar, Jan Martin Nordbotten, Iuliu Sorin Pop*, **Analysis of a linearization scheme for an interior penalty discontinuous Galerkin method for two phase flow in porous media with dynamic capillarity effects** , 2016

UP-16-03 *Sergey Alyaev, Eirik Keilegavlen, Jan Martin Nordbotten, Iuliu Sorin Pop*, **Fractal structures in freezing brine**, 2016

UP-16-02 *Klaus Kaiser, Jochen Schütz, Ruth Schöbel and Sebastian Noelle*, **A new stable splitting for the isentropic Euler equations**, 2016

UP-16-01 *Jochen Schütz and Vadym Aizinger*, **A hierarchical scale separation approach for the hybridized discontinuous Galerkin method**, 2016